complexes analogous to the distorted octahedral cobalt(II) boranecarboxylate complex (**3**) have been reported with magnetic moments in the range of 4.93-5.15 μ_B, similar to the one reported here.[29]

Summary

This study unequivocally supports the proposed formulation for complexes **2-5** showing that the trimethylamine-boranecarboxylato ligand (**1'**) behaves similarly to organic carboxylato ligands, acting as a monodentate (**2**) and bidentate chelating ligand (**3-5**). The biological activity of these compounds is currently under investigation.

Acknowledgment. The authors express their gratitude to the Utah State University Research Office for its financial support and to Dr. D. G. Holah for elemental analyses. USU Provost's and President's Fellowships as well as a Sigma Xi Research Award to V.M.N. are also gratefully acknowledged.

(29) Johnson, S. A.; Hunt, H. R.; Newmann, H. M. *Inorg. Chem.* **1963**, *2*, 960.

Contribution from the Departments of Chemistry, Stanford University, Stanford, California 94305, Dartmouth College, Hanover, New Hampshire 03755, and Franklin and Marshall College, Lancaster, Pennsylvania 17604

Polarized, Single-Crystal, Electronic Spectral Studies of $Cu_2Cl_6^{2-}$: Excited-State Effects of the Binuclear Interaction

Sylvie R. Desjardins,[1a] Dean E. Wilcox,[1a,b] Ronald L. Musselman,[1c] and Edward I. Solomon*[1a]

Received July 7, 1986

Variable-temperature, polarized, single-crystal, electronic spectra (10 000-45 000 cm^{-1}) have been taken on a series of mononuclear ($(CH_3NH_3)_2CuCl_4$, $(C_2H_5NH_3)_2CuCl_4$, and (*N*-(2-ammonioethyl)piperazinium)$CuCl_5 \cdot 2H_2O$) and binuclear ($KCuCl_3$, $(CH_3)_2NH_2CuCl_3$, and $LiCuCl_3 \cdot 2H_2O$) chlorocuprates in order to evaluate the excited-state effects of the binuclear cupric interaction. The increased intensity in the ligand field region of the binuclear complexes, relative to that of the monomers, has been shown to arise from the lower single-ion site symmetry in the dimer structure, which causes certain ligand field transitions to become parity allowed in a lower site symmetry. Attention is particularly focused on the absorption bands present in the dimers at ~20 000 cm^{-1}, which are not present in the analogous monomers, and the intensity, polarization, temperature dependence, and band shape of these "dimer" bands in the three binuclear cupric complexes have been studied in detail. We have experimentally evaluated the two possible assignments for these spectral features: simultaneous pair excitations (SPE; one photon excitation of ligand field transitions on both Cu(II)'s) and chloride-to-copper(II) charge-transfer transitions, which appear at 3700 cm^{-1} lower energy than in the analogous monomer. The temperature dependence of the dimer band intensity correlates with the population of the ground-state singlet, indicating that this is a singlet-to-singlet excitation. The polarization and, in particular, the band shape of this feature show that it should be assigned as the singlet component of a nonbonding π charge-transfer transition and not a SPE transition. The corresponding triplet-to-triplet excitation is estimated to have comparable intensity, yet it is not observed within the accessible spectral region below the intense charge-transfer cutoff. This charge-transfer triplet is thus required to be at least 3000 cm^{-1} to higher energy than the singlet. The large stabilization of this charge-transfer singlet, compared to that of the corresponding triplet, can be associated with a large antiferromagnetic excited-state exchange coupling relative to the ground-state exchange coupling in the binuclear complexes.

Introduction

The goal of numerous experimental[2] and theoretical[3] studies of binuclear Cu(II) complexes has been to explain the molecular ground-state properties resulting from the binuclear interactions. The observed antiferromagnetic or ferromagnetic behavior is usually described by a spin Hamiltonian involving exchange interaction between the Cu(II) valence electrons leading to a singlet ($S_{tot} = 0$) and a triplet ($S_{tot} = 1$) spin state. The molecular orbital or valence bond descriptions, however, generally include[3] configurational interaction between the ground state and a Cu(II) $\rightarrow$ Cu(II) charge-transfer excited state in order to achieve the experimentally observed sign and magnitude of the singlet-triplet splitting $2J$.

The binuclear interaction also has a direct effect on the excited states, as seen[4] in the optical spectra of binuclear Cu(II) complexes. While intensity enhancement of spin-forbidden ligand field transitions is well-known and studied in Mn(II)[5] and Cr(III)[6] dimers, the spin-allowed ligand field transitions of Cu(II) dimers are also observed to be more intense. Perhaps most striking is the appearance in the dimers of new transitions in a near-UV or visible spectral region that is transparent in the monomers. These dimer bands have generated a number of spectral studies and possible assignments, especially for the binuclear cupric carboxylate systems.[7] Finally, although not yet evaluated relative to the spectra of the monomers, the charge-transfer spectrum would also be expected to be strongly influenced by binuclear effects.

In order to experimentally characterize the effects of binuclear interaction on the excited states of copper(II) dimers, we have undertaken a detailed spectroscopic study of a series of binuclear chlorocuprates.[8] This series, containing a simple homogeneous ligand set, was chosen for a number of reasons. First, structurally characterized monomeric analogues exist for spectral comparison and their ligand field[9] and charge-transfer[10] spectra have been studied in detail through polarized, single-crystal methods. Second, while the dimer bands of binuclear Cu(II) complexes, such as

* To whom all correspondence should be addressed.

(1) (a) Stanford University. (b) Dartmouth College. (c) Franklin and Marshall College.
(2) *Magneto-Structural Correlations in Exchange Coupled Systems*; Willett, R. D., Gatteschi, D., Kahn, O., Eds.; D. Reidel: Dordrecht, The Netherlands, 1985.
(3) (a) Anderson, P. W. *Phys. Rev.* **1959**, *115*, 2-13. (b) Hay, P. J.; Thibeault, J. C.; Hoffmann, R. *J. Am. Chem. Soc.* **1975**, *97*, 4884-4899.
(4) (a) Willett, R. D.; Liles, O. L., Jr. *Inorg. Chem.* **1967**, *6*, 1666-1669. (b) Dubicki, L. *Aust. J. Chem.* **1972**, *25*, 1141-1149.
(5) Ferguson, J.; Guggenheim, H. J.; Tanabe, Y. *J. Phys. Soc. Jpn.* **1966**, *21*, 692-704.
(6) Decurtins, S.; Gudel, H. U. *Inorg. Chem.* **1982**, *21*, 3598-3606 and references therein.
(7) (a) Kida, S.; Nakashima, Y.; Morimoto, Y.; Nimi, K.; Yamada, S. *Bull. Chem. Soc. Jpn.* **1964**, *37*, 549. (b) Hansen, A. E.; Ballhausen, C. J. *Trans. Faraday Soc.* **1965**, *61*, 631-639. (c) Dubicki, L.; Martin, R. L. *Inorg. Chem.* **1966**, *5*, 2203-2209.
(8) Smith, D. W. *Coord. Chem. Rev.* **1976**, *21*, 93-158.
(9) (a) Hitchman, M. A.; Cassidy, P. J. *Inorg. Chem.* **1979**, *18*, 1745-1754. (b) Hitchman, M. A.; Cassidy, P. J. *Inorg. Chem.* **1978**, *17*, 1682-1685.
(10) Desjardins, S. R.; Penfield, K. W.; Cohen, S. L.; Musselman, R. L.; Solomon, E. I. *J. Am. Chem. Soc.* **1983**, *105*, 4590-4603.

0020-1669/87/1326-0288$01.50/0

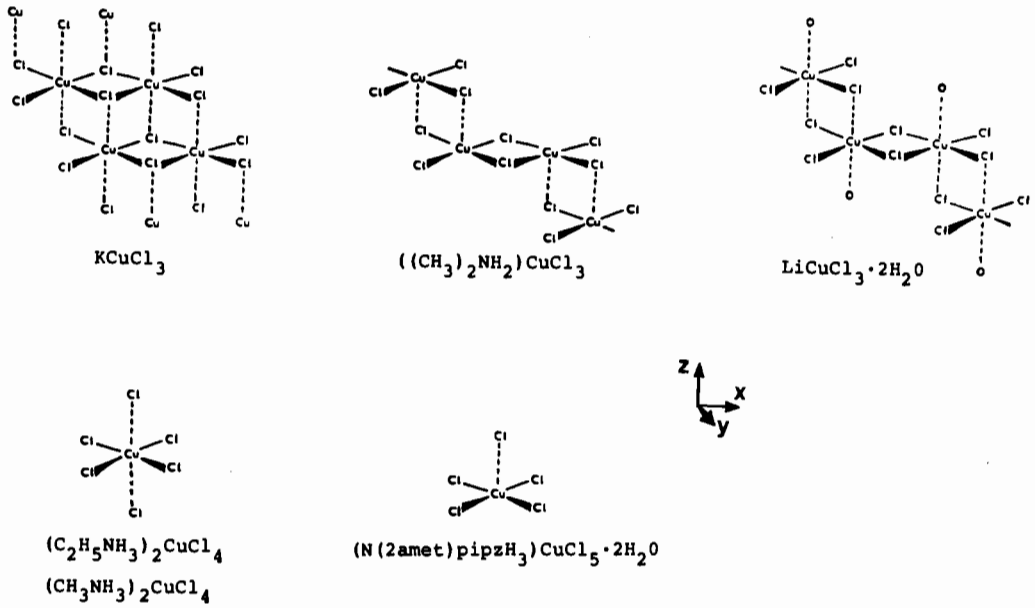

Figure 1. Representations of the mononuclear and binuclear chlorocuprate single-crystal structures.

$Cu_2(OAc)_4 \cdot 2H_2O$, are often in the near-UV region and are difficult to resolve[4b] due to overlap with intense higher energy charge-transfer transitions, in the binuclear chlorocuprates these bands are in the visible region ($\sim$20 000 cm^{-1}), well-separated in energy from the charge-transfer transitions; this allows them to be studied with minimum interference from more intense optical features. Third, the ground-state exchange splittings in the chlorocuprate series are relatively small ($|2J| < 100$ cm^{-1}) and variations in the sign and magnitude are associated[11] with limited structural differences among the binuclear complexes. As a further consequence of this relatively small exchange coupling, changes in the populations of the ground spin states will occur at low temperatures (<100 K), where changes in vibronic coupling no longer affect optical transition intensities and thereby complicate other spectral contributions.

Figure 1 gives the coordination geometries of the mononuclear and binuclear chlorocuprates of this study. The key dimer structure is the planar $Cu_2Cl_6^{2-}$ binuclear unit. In $KCuCl_3$, the tetragonal symmetry[12] at each copper(II) includes two additional axial Cl^- ligands at $\sim$3.0 Å, which belong to the equatorial plane of adjacent binuclear units. The complexes $(C_2H_5NH_3)_2CuCl_4$ and $(CH_3NH_3)_2CuCl_4$ have a similar coordination geometry[13] (four short strongly bound equatorial Cl^- ligands and two longer weakly bound axial Cl^-'s) and have been studied as tetragonal mononuclear analogues. The complex $((CH_3)_2NH_2)CuCl_3$ retains the binuclear $Cu_2Cl_6^{2-}$ unit;[14] however, each copper now has only a single axial Cl^- ligand provided by an adjacent binuclear unit. This square-pyramidal geometry around the individual coppers and the stacking of the dimers result in a somewhat distorted $Cu_2Cl_6^{2-}$ unit with the coppers displaced toward the axial chloride. We have studied this binuclear chlorocuprate and the complex (*N*-(2-ammonioethyl)piperazinium)pentachlorocopper(II) dihydrate ($(N(2amet)pipzH_3)CuCl_5 \cdot 2H_2O$), which provides an analogous mononuclear square-pyramidal geometry[15] for comparison. Finally, although there exists no appropriate monomeric analogue, we have included $LiCuCl_3 \cdot 2H_2O$ in this study. Its crystal structure[16] contains the nearly planar $Cu_2Cl_6^{2-}$ binuclear unit; however, axial ligation of each copper now includes one Cl^- from an adjacent dimer and one OH_2 water of hydration.

We have taken polarized, single-crystal, variable-temperature absorption spectra of these six chlorocuprate salts to obtain detailed information about the ligand field transitions and dimer band spectral region. We also report polarized, single-crystal, specular reflectance data on the UV charge-transfer transitions of the {010} faces of $KCuCl_3$. These spectral data provide important new insight about the origin of the increased intensity in the ligand field region and, in particular, the assignment of the dimer band of binuclear cupric complexes.

Experimental Section

Six different chlorocuprate salts were studied by linearly polarized absorption and specular reflectance spectroscopies using instrumentation and procedures as outlined in our earlier study[10] of the charge-transfer spectra of mononuclear chlorocuprates. The preparation, morphology, and polarization properties of the mononuclear complexes $(C_2H_5NH_3)_2CuCl_4$ and $(CH_3NH_3)_2CuCl_4$ have been previously indicated.[10]

Single crystals[12] of $KCuCl_3$ were grown from a concentrated HCl solution saturated with KCl and $CuCl_2 \cdot 2H_2O$ in the ratio of 1:4, which was allowed to evaporate for weeks over Drierite in a closed but not evacuated desiccator. For the resulting dark red needles with hexagonal cross sections, the needle axis is *a* of the $P2_1/c$ unit cell and one pair of predominant faces is {010}, which exhibits a 2-symmetry plane interference figure; the other two pairs are {011} and {01$\bar{1}$}. Polarized absorption spectra were taken of *ac* and *ab* sections; polishing of the latter required mounting the crystal on a ridge. The extinction directions of the {010} faces are located at +52° (red) and −38° (yellow) to the *a* axis, the + sign corresponding to a rotation of the electric vector into the quadrant containing the obtuse angle. There is no variation of the *ac* extinction directions as a function of either wavelength or temperature. Defining a molecular coordinate system based on the approximate D_{2h} symmetry of the nearly planar $Cu_2Cl_6^{2-}$ ion, with *X* along the Cu–Cu direction, *Y* orthogonal to *X* and in the equatorial plane, and *Z* normal to the *XY* plane, the following relationships are obtained:

$$I_{red} = 0.823I_X + 0.176I_Y + 0.001I_Z$$

$$I_{yellow} = 0.018I_X + 0.052I_Y + 0.930I_Z$$

$$I_a = 0.213I_X + 0.194I_Y + 0.593I_Z$$

$$I_b = 0.159I_X + 0.772I_Y + 0.070I_Z$$

Molecular polarized absorption data were obtained with the red, yellow, and *b* crystal polarizations as they each have one dominant molecular polarization component; this set thus tends to minimize thickness measurement errors in determining the molar extinction values.

(11) Willett, R. D. In ref 2, pp 389–420.
(12) Willett, R. D.; Dwiggins, C., Jr.; Kruh, R. F.; Rundle, R. E. *J. Chem. Phys.* **1963**, *38*, 2429–2436.
(13) (a) Steadman, J. P.; Willett, R. D. *Inorg. Chim. Acta* **1970**, *4*, 367–371. (b) Arend, H.; Huber, W.; Mischgofsky, F. H.; Richter-van Leeuwen, G. K. *J. Cryst. Growth* **1978**, *43*, 213. (c) Willett, R. D. *J. Chem. Phys.* **1964**, *41*, 2243–2244.
(14) Willett, R. D. *J. Chem. Phys.* **1966**, *44*, 39–42.
(15) Antolini, L.; Marcotrigiano, G.; Menabue, L.; Pellacani, G. C. *J. Am. Chem. Soc.* **1980**, *102*, 1303–1309.
(16) Vossos, P. H.; Fitzwater, D. R.; Rundle, R. E. *Acta Crystallogr.* **1963**, *16*, 1037–1045.

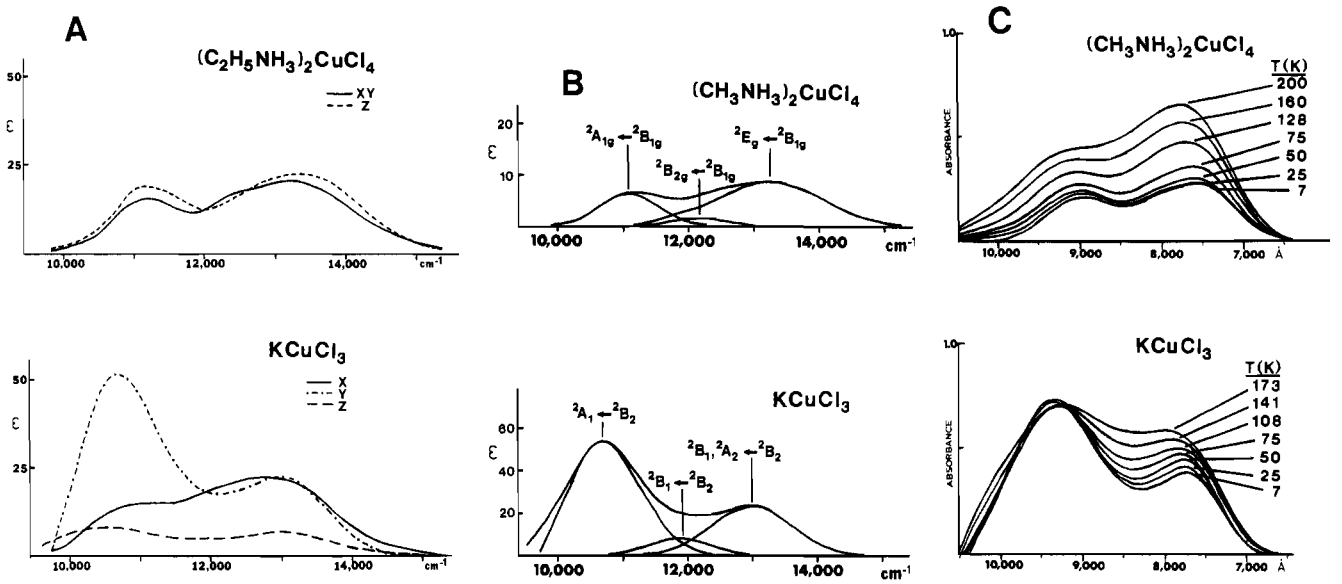

Figure 2. (A) Molecular polarized absorption spectra: (upper) $(C_2H_5NH_3)_2CuCl_4$ (10 K; adapted from ref 9b); (lower) $KCuCl_3$ (7 K). (B) Gaussian resolved spectra: (upper) $(CH_3NH_3)_2CuCl_4$ (*bc* face E$\|c$; 52% *Z* and 48% *X,Y*; 7 K); (lower) $KCuCl_3$ (*Y*-polarized spectrum from (A), 7 K). Band assignments (see text) are in D_{4h} and C_{2v}, respectively. (C) Temperature-dependent spectra: (upper) $(CH_3NH_3)_2CuCl_4$ (*bc* face E$\|c$; 52% *Z* and 48% *X,Y*); (lower) $KCuCl_3$ (*ab* face E$\|a$; 21% *X*, 19% *Y*, 59% *Z*).

Polarized, single-crystal, specular reflectance spectra were taken along the extinction directions of the $KCuCl_3$ {010} faces, and polarized absorption spectra were obtained through Kramers–Kronig transformation of these reflectance data. An effective transition is added in the vacuum-UV region to provide the reflectivity necessary for proper base line behavior throughout the experimental region upon transformation.[10] The intensity of this effective band was adjusted to give minimum absorption at the low-energy side of the $KCuCl_3$ charge-transfer spectrum, where absorption spectra show no intensity. This adjustment does not affect the energies of transformed absorption bands.

Single crystals of (*N*-(2-ammonioethyl)piperazinium)pentachlorocopper(II) dihydrate (hereafter referred to as $(N(2amet)pipzH_3)CuCl_5 \cdot 2H_2O$) were grown by slow evaporation of the dark green acidic aqueous ethanolic solution prepared by the method of Antolini et al.[15] Precession photographs identified the {100} and {001} faces of the yellow-green monoclinic crystals (typically 1 mm × 3 mm × 5 mm), which belong to the $P2_1/a$ space group. Spectra were taken parallel and perpendicular to *b* on both the *bc* and a^*b faces, where $a^* \perp c$; the latter was obtained by polishing the *ab* face. The four $CuCl_5^{3-}$ anions per unit cell are square pyramids with the Cu(II) displaced 0.30 Å out of the equatorial plane toward the axial Cl^-. While two coordinate systems can be chosen for this square-pyramidal $CuCl_5^{3-}$ structure, molecularly polarized spectra with *X* and *Y* being perpendicular to the $Cu-Cl_{ax}$ bond and oriented in the direction of the $Cu-Cl_{eq}$ bonds gave negative intensities for the *Z*-polarized spectra. Therefore, the alternative coordinate system with *X* and *Y* oriented in the direction of the bisectors of the $Cl_{eq}-Cu-Cl_{eq}$ angles was used, leading to the polarization relationships

$$I_{a'} = 0.045I_X + 0.759I_Y + 0.196I_Z$$

$$I_b = 0.161I_X + 0.241I_Y + 0.599I_Z$$

$$I_c = 0.794I_X + 0.000I_Y + 0.206I_Z$$

Well-formed, single crystals[14] of $((CH_3)_2NH_2)CuCl_3$ were grown by allowing a 1:1 solution of $(CH_3)_2NH \cdot HCl$ and $CuCl_2 \cdot 2H_2O$ in ethanol to evaporate slowly. The long axis of these red monoclinic ($I2/a$ space group) crystals is *a*, and the predominant faces are {001}, {011}, and {01$\bar{1}$}. Polishing of the *ac* section now required mounting the crystal on a ridge, and the extinction directions of this face are located at +22.5° (red) and −67.5° (green) to the *a* axis. Defining the same molecular coordinate system used for $KCuCl_3$, the following equations are obtained for $((CH_3)_2NH_2)CuCl_3$:

$$I_{red} = 0.658I_X + 0.326I_Y + 0.015I_Z$$

$$I_{green} = 0.001I_X + 0.064I_Y + 0.935I_Z$$

$$I_a = 0.578I_X + 0.184I_Y + 0.237I_Z$$

$$I_b = 0.341I_X + 0.610I_Y + 0.050I_Z$$

As for $KCuCl_3$, the red, green, and *b* crystal polarizations were used in determining the molecular polarizations. On the basis of the chosen molecular coordinate system, *Y* is the unique C_{2h} symmetry axis of this structure.

Single crystals[16] of $LiCuCl_3 \cdot 2H_2O$ were grown by evaporating, under dry room conditions, an aqueous solution containing a 3:1 ratio of LiCl to $CuCl_2 \cdot 2H_2O$. The brownish red needles of large hexagonal cross section have *a* as the needle axis, and {010}, {011}, and {01$\bar{1}$} are the predominant faces. Extinction directions of the *ac* face are located at +60.5° (yellow) and −29.5° (red) to the *a* axis and do not vary as a function of either wavelength or temperature. From the consistent $Cu_2Cl_6^{2-}$ molecular coordinate system, the following equations are obtained for $LiCuCl_3 \cdot 2H_2O$:

$$I_{red} = 0.991I_X + 0.000I_Y + 0.009I_Z$$

$$I_{yellow} = 0.007I_X + 0.279I_Y + 0.714I_Z$$

$$I_a = 0.674I_X + 0.072I_Y + 0.254I_Z$$

$$I_b = 0.002I_X + 0.721I_Y + 0.277I_Z$$

Once again, the molecular polarizations were determined from the red, yellow, and *b* crystal polarizations, and the unique C_{2h} axis is *Y*.

Results and Analysis

Ligand Field Transitions. Variable-temperature, polarized, single-crystal, absorption spectra have been taken in the 10 000–15 000 cm^{-1} region of the three binuclear and the three mononuclear chlorocuprates included in this study. While these spectra of the ligand field transitions (Figures 2–4) are described in detail below, we initially note that the total envelope of ligand field transitions in the binuclear complexes shows no significant shift in energy upon comparison to those of the analogous mononuclear structures. This is consistent with the similar ligand fields around the copper(II) ions in the comparable mononuclear and binuclear complexes. Within the envelope of ligand field transitions, however, the binuclear complexes have different intensity distributions relative to those of the analogous monomers and in particular a significant increase in intensity appears on the low-energy side of the $KCuCl_3$ spectrum.

$KCuCl_3$. Figure 2 shows the low-temperature, molecular-polarized, absorption spectra (Figure 2A) of $(C_2H_5NH_3)_2CuCl_4$ and $KCuCl_3$, as well as the Gaussian resolution (Figure 2B) and temperature dependence (Figure 2C) of the $(CH_3NH_3)_2CuCl_4$ and $KCuCl_3$ spectra. Examination of this data reveals several important observations. Not only is there no major shift in the dimer envelope of ligand field transitions (Figure 2A), but the $KCuCl_3$ absorption envelope can be deconvoluted into three Gaussian bands (Figure 2B; Table I) at energies that are similar to those obtained and previously assigned[17] for the mononuclear

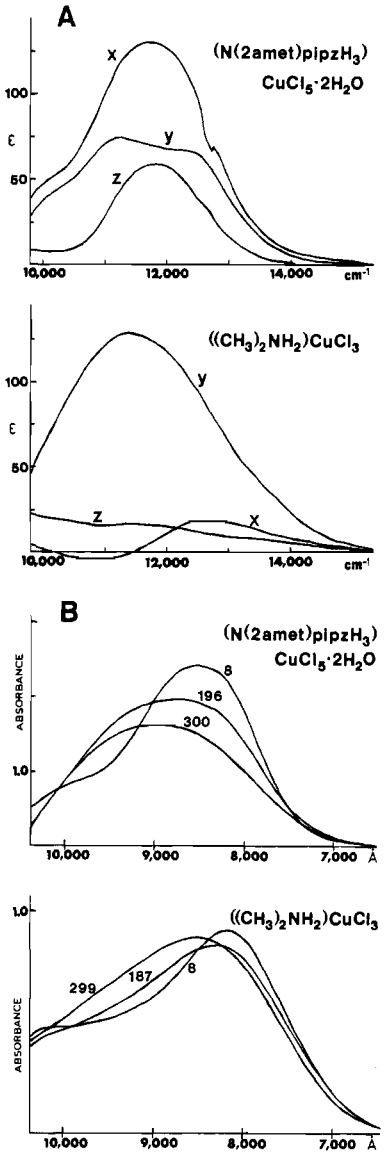

Figure 3. (A) Molecular-polarized absorption spectra (8 K): (upper) $(N(2amet)pipzH_3)CuCl_5 \cdot 2H_2O$; (lower) $((CH_3)_2NH_2)CuCl_3$. (B) Temperature-dependent spectra: (upper) $(N(2amet)pipzH_3)CuCl_5 \cdot 2H_2O$ (*bc* face E‖*c*; 79% *X* and 21% *Z*); (lower) $((CH_3)_2NH_2)CuCl_3$ (*ac* face E‖red; 66% *X*, 33% *Y*, 1% *Z*).

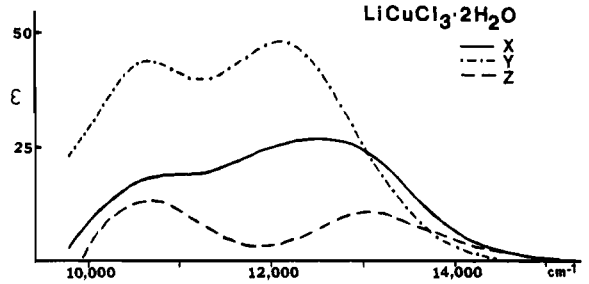

Figure 4. Molecular-polarized absorption spectra of $LiCuCl_3 \cdot 2H_2O$ (7 K).

complexes. Thus, the individual Cu(II) ligand field energy levels are not significantly shifted by the binuclear interaction and, within the limits of the Gaussian analysis, there is no resolvable splitting

(17) The assignment[9] of the mononuclear, tetragonal chlorocuprate ligand field transitions has the unpaired electron in a $d_{x^2-y^2}$ orbital and thus a $^2B_{1g}$ (in D_{4h}) ground state. The molecular coordinate system used in this study of the binuclear chlorocuprates has the *X* and *Y* axes rotated by 45°, and therefore the unpaired electron of the individual Cu(II)'s is in a d_{xy} orbital with a $^2B_2$ (in C_{2v}) ground state.

Table I. Gaussian Analysis of the Envelope of Ligand Field Transitions for Mononuclear and Binuclear Tetragonal Chlorocuprates

	transition energy, cm^{-1} (fwhm, cm^{-1})		
complex	$a_{1g}(d_{z^2}) \rightarrow b_{1g}(d_{x^2-y^2})$	$b_{2g}(d_{xy}) \rightarrow b_{1g}(d_{x^2-y^2})$	$e_g(d_{xz},d_{yz}) \rightarrow b_{1g}(d_{x^2-y^2})$
$(C_2H_5NH_3)_2CuCl_4$ (*XY* polarizn, 8 K)	10 990 (1200)	12 100 (1100)	13 250 (1660)
$(CH_3NH_3)_2CuCl_4$ (48% *XY* and 52% *Z* polarizn, 7 K)	11 090 (1070)	12 110 (1070)	13 210 (1950)
$KCuCl_3$ (*Y* polarizn, 7 K)	10 700 (1360)	11 850 (1260)	12 950 (1400)

of these transitions in the binuclear electronic structure. For $KCuCl_3$, the higher intensity of the binuclear ligand field transitions is found to be dominantly associated with the lower energy transition, corresponding to the $a_{1g}(d_{z^2}) \rightarrow b_{1g}(d_{x^2-y^2})$ transition in the monomer, and to be strongly *Y* polarized. Further, the *Z*-polarized intensity is observed to be low in the binuclear complex.

The temperature dependence of the dimer transitions (Figure 2C, bottom) reflects two different intensity mechanisms. The higher energy binuclear transition, corresponding to the 13 250-cm^{-1} $e_g(d_{xz},d_{yz}) \rightarrow b_{1g}(d_{x^2-y^2})$ transition in the monomer, shows a decrease in intensity upon cooling, which parallels the behavior of all the monomer transitions (Figure 2C, top). We have analyzed the monomer ligand field transitions in more detail, and using a vibronic coupling intensity mechanism, we have fit the temperature dependence of the integrated intensity ($f(T)$) of the absorption envelope of the $(CH_3NH_3)_2CuCl_4$ ligand field transitions to the relationship[18]

$$f(T) = f(7\text{ K}) \coth (\nu_i/2kT)$$

This analysis yields an effective vibrational frequency (ν_i) of 104 cm^{-1}, which is a reasonable value for vibronic coupling in mononuclear Cu(II) complexes. An analogous fit of the higher energy $KCuCl_3$ ligand field band to this vibronic coupling mechanism gives an effective vibrational frequency (ν_i) of 43 cm^{-1}. While this lower value may reflect a decrease in the effective odd-parity vibrational frequency in the dimer structure, this difference is more likely due to error in accurately determining the integrated intensity of this $KCuCl_3$ band within the total envelope of ligand field transitions. In either case, the general increase in intensity with increasing temperature indicates that a vibronic coupling mechanism still provides intensity for the higher energy, parity-forbidden, $^2E_g \leftarrow {}^2B_{1g}$ monomer ligand field transition in the binuclear structure. The lower energy, more intense, *Y*-polarized, ligand field band of $KCuCl_3$, however, retains its intensity and sharpens (decreased bandwidth) upon cooling; this behavior indicates that the lowest energy d → d transition in the D_{4h} monomer, $^2A_{1g} \leftarrow {}^2B_{1g}$, becomes parity-allowed in the dimer.

Table IIA shows the ground-state single-ion transitions, excited states, and transition polarizations for the C_{2v} monomer site ($C_2 = X$) within the binuclear complex and the ground states, excited states, and transition polarizations obtained in a coupled-chromophore analysis of the D_{2h} tetragonal $Cu_2Cl_6^{2-}$ dimer. In the coupled-chromophore model, as given by Hansen and Ballhausen[7b] for $Cu_2(OAc)_4 \cdot 2H_2O$, the symmetries of the symmetric and antisymmetric combinations of Cu(II) monomer valence levels in the ground state and one-electron, ligand field, excited states are used to determine the symmetries of the singlet and triplet dimer states.

Comparing the polarization, intensity, and temperature dependence of the $KCuCl_3$ data in Figure 2 and the analysis in Table IIA, we find that the low-energy, *Y*-polarized transition in $KCuCl_3$, which corresponds to the $a_{1g}(d_{z^2}) \rightarrow b_{1g}(d_{x^2-y^2})$ transition in the monomer, is predicted to be the parity-allowed, *Y*-polarized $a_1(d_{z^2}) \rightarrow b_2(d_{xy})$ transition in the C_{2v} single-ion site. Thus, we find an additional intensity mechanism associated with the lower symmetry

(18) Liehr, A. D.; Ballhausen, C. J. *Phys. Rev.* **1957**, *106*, 1161–1163.

Table II. Single-Ion Ligand Field Transitions and Coupled-Chromophore Analysis

A. Tetragonal $Cu_2Cl_6^{2-}$

	monomer (C_{2v}) $^2B_2$ (ground state)		dimer (D_{2h}) ^1A_g, $^3B_{3u}$ (ground state)	
single-ion transitions	excited state	polarizn	excited states	polarizn
$a_1 \rightarrow b_2$ ($z^2 \rightarrow xy$)	$^2A_1$	y	$^1B_{1g}$, $^1B_{2u}$, $^3B_{1g}$, $^3B_{2u}$	y
$a_1 \rightarrow b_2$ ($x^2 - y^2 \rightarrow xy$)	$^2A_1$	y	$^1B_{1g}$, $^1B_{2u}$, $^3B_{1g}$, $^3B_{2u}$	y
$b_1 \rightarrow b_2$ ($xz \rightarrow xy$)	$^2B_1$		$^1B_{3g}$, ^1A_u, $^3B_{3g}$, ^3A_u	
$a_2 \rightarrow b_2$ ($yz \rightarrow xy$)	$^2A_2$	z	$^1B_{2g}$, $^1B_{1u}$, $^3B_{2g}$, $^3B_{1u}$	z

B. Square-Pyramidal $Cu_2Cl_6^{2-}$

	monomer (C_s) $^2A''$ (ground state)		dimer (C_{2h}) ^1A_g, ^3B_u (ground state)	
single-ion transitions	excited state	polarizn	excited states	polarizn
$a' \rightarrow a''$ ($z^2 \rightarrow xy$)	$^2A'$	y	^1B_g, ^1A_u, ^3B_g, ^3A_u	y
$a' \rightarrow a''$ ($x^2 - y^2 \rightarrow xy$)	$^2A'$	y	^1B_g, ^1A_u, ^3B_g, ^3A_u	y
$a' \rightarrow a''$ ($xz \rightarrow xy$)	$^2A'$	y	^1B_g, ^1A_u, ^3B_g, ^3A_u	y
$a'' \rightarrow a''$ ($yz \rightarrow xy$)	$^2A''$	x,z	^1A_g, ^1B_u, ^3A_g, ^3B_u	x,z

Cu(II) monomer site in the dimer, and this low site symmetry leads to the increased and temperature-independent Y-polarized intensity for this transition. The $b_{2g}(d_{xy}) \rightarrow b_{1g}(d_{x^2-y^2})$ transition at $\sim$12 000 cm^{-1} in the monomer is quite weak; the analogous transition in the dimer has more intensity (Figure 2B), consistent with that predicted for the parity-allowed, Y-polarized $a_1(d_{x^2-y^2}) \rightarrow b_2(d_{xy})$ transition (Table IIA). However, since this band is only resolved in the Gaussian analysis and is strongly overlapped with other transitions showing vibronic and sharpening behavior upon cooling, the temperature dependence of this transition cannot be determined. While it may show some vibronic behavior, the increased intensity of this band at low temperature is consistent with this assignment in the single-ion C_{2v} site of the dimer. As indicated previously, the highest energy $KCuCl_3$ ligand field band, which corresponds to the $e_g(d_{xz},d_{yz}) \rightarrow b_{1g}(d_{x^2-y^2})$ monomer transition, shows a vibronic temperature dependence. In the C_{2v} monomer site of the dimer, this band corresponds (Table IIA) to a combination of the $b_1(d_{xz}) \rightarrow b_2(d_{xy})$ transition, which is electric-dipole-forbidden in this single-ion site, and the $a_2(d_{yz}) \rightarrow b_2(d_{xy})$ transition, which is predicted to have Z-polarized intensity. However, the lack of Z intensity (Figure 2A, bottom) associated with this latter transition is consistent with the fact that in the charge-transfer spectrum there is no Z-polarized intensity (vide infra), which would be required for second-order perturbation mixing into the $^2A_2 \leftarrow {}^2B_2$ transition. Thus, both of these dimer transitions are predicted to show only vibronic temperature-dependent behavior, as observed for the highest energy $KCuCl_3$ ligand field band.

The electronic structure of the binuclear complex, as indicated by the coupled-chromophore analysis, could perturb the single Cu(II) ion ligand field energy levels, leading to splittings of the d–d transitions; the intensities of the ligand field transitions and their temperature dependence could also be affected by configurational interaction between states of the binuclear electronic structure. However, the experimentally observed differences (Figure 2) between the ligand field transitions in the mononuclear and binuclear tetragonal chlorocuprates can be simply explained as arising from the lower symmetry of the single Cu(II) site in the dimer structure. In particular, we find no evidence for unusual temperature-dependent behavior of the ligand field transitions, especially in the 7–77 K region, which would be associated with changes in the ground-state singlet and triplet populations and which would reflect new dimer intensity mechanisms as observed for the dimer bands (vide infra).

$((CH_3)_2NH_2)CuCl_3$. Figure 3 shows the low-temperature, molecular-polarized, absorption spectra (Figure 3A) of (N-(2amet)pipzH$_3$)$CuCl_5 \cdot 2H_2O$ and $((CH_3)_2NH_2)CuCl_3$, as well as the temperature dependence of these spectra (Figure 3B). The ligand field transition envelopes for these two complexes are at very similar energies, and there is little difference in transition intensity between the monomer and the dimer. Further, the transition intensity in these two complexes shows similar temperature-dependent behavior: while there is some sharpening of the bands, the total intensity changes very little upon cooling. Thus, the intensity of the ligand field transitions in both the monomer and dimer complexes is governed by an odd-parity, static distortion mechanism.

A spectroscopic difference between the square-pyramidal monomer and dimer is observed in the polarizations of the ligand field transitions; (N(2amet)pipzH$_3$)$CuCl_5 \cdot 2H_2O$ shows unequal mixed polarization of its ligand field transitions,[19] while $((CH_3)_2NH_2)CuCl_3$ has most of its ligand field intensity in the molecular Y polarization. An examination of the Cu(II) site symmetry in these two complexes indicates the origin of this polarization difference. For a C_{4v} mononuclear complex, the highest energy transition $e(d_{xz},d_{yz}) \rightarrow b_2(d_{xy})$ is predicted to be parity-allowed and X,Y-polarized; this transition is the major component in the envelope of square-pyramidal monomer and dimer ligand field transitions seen in Figure 3. Lowering the monomer Cu(II) symmetry to C_{2v} removes the degeneracy of d_{xz} and d_{yz} and splits the X ($b_1(d_{xz}) \rightarrow a_2(d_{xy})$) and Y ($b_2(d_{yz}) \rightarrow a_2(d_{xy})$) polarized transitions. However, the appearance of significant Z-polarized intensity requires an even lower symmetry. The spectroscopic effective site symmetry of this square-pyramidal monomeric complex can thus be considered to be the crystallographic[15] C_1 symmetry. In $((CH_3)_2NH_2)CuCl_3$, the dimer structure[14] has an ideal C_{2h} symmetry (see Figure 1), while the single Cu(II) site within the dimer has an effective C_s symmetry (XZ is the reflection plane). The ground-state, single-ion ligand field transitions, excited states, and transition polarizations of this C_s monomer site in the dimer molecule are given in Table IIB; also included in this table are the ground states, excited states, and ligand field transition polarizations from a coupled-chromophore analysis of the C_{2h} square-pyramidal $Cu_2Cl_6^{2-}$ dimer. Most ligand field transitions of the C_s monomer site are predicted to be electric-dipole-allowed in Y polarization. The $a'(d_{xz}) \rightarrow a''(d_{xy})$ and $a'(d_{x^2-y^2}) \rightarrow a''(d_{xy})$ transitions, therefore, appear to contribute the dominant, Y-polarized intensity to the envelope of $((CH_3)_2NH_2)CuCl_3$ ligand field transitions (Figure 3A, bottom); the weak X intensity on the high-energy side of the envelope may be associated with the $a''(d_{yz}) \rightarrow a''(d_{xy})$ transition. The change in the polarization properties of the ligand field transitions from unequal mixed polarization in the monomeric complex to dominantly Y intensity in the binuclear structure is thus a consequence of the change in the effective Cu(II) single-ion site symmetry from C_1 in the monomer to C_s in the dimer. While the observed spectra

(19) Recent diffuse reflectance data for (N(2amet)pipzH$_3$)$CuCl_5 \cdot 2H_2O$ (Reinen, D.; Friebel, C. *Inorg. Chem.* **1984**, *23*, 791–798) shows, in addition to the dominant intensity centered at 11 500 cm^{-1}, low-energy shoulders at 8200 and 10 000 cm^{-1}, which are assigned in C_{4v} symmetry as the ligand field transitions $^2A_1(z^2) \leftarrow {}^2B_1(x^2 - y^2)$ and $^2B_2(xy) \leftarrow {}^2B_1(x^2 - y^2)$, respectively. Our data show the latter feature as well as the dominant band, which corresponds to the $^2E(xz,yz) \leftarrow {}^2B_1(x^2 - y^2)$ transition.

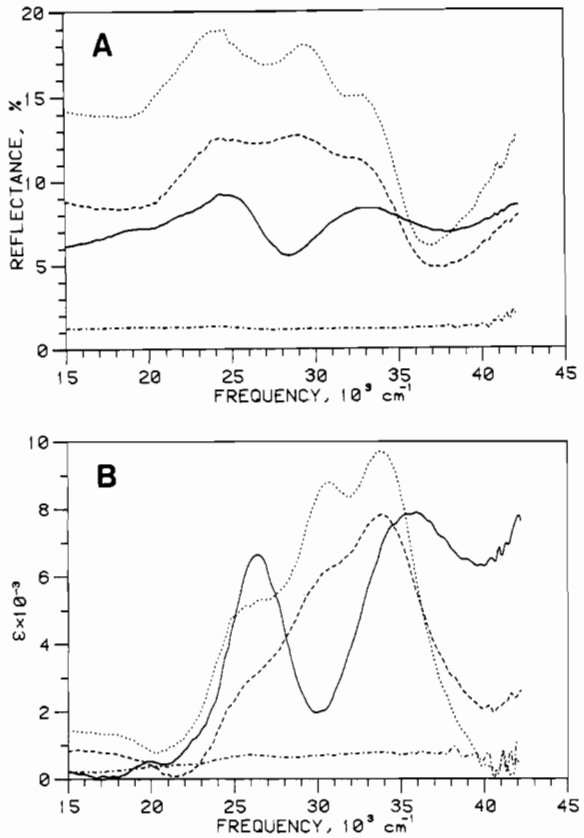

Figure 5. Polarized single-crystal (A) specular reflectance spectra and (B) Kramers–Kronig transformed absorption spectra (molar extinction values per $CuCl_4^{2-}$ and $Cu_2Cl_6^{2-}$): (—) $(C_2H_5NH_3)_2CuCl_4$, *bc* face, E‖*c* (48% *X*,*Y* and 52% *Z*), room temperature; (- - -) $KCuCl_3$, *ac* face, E‖red (82% *X* and 18% *Y*), room temperature; (-·-) $KCuCl_3$, *ac* face, E‖yellow (2% *X*, 5% *Y*, 93% *Z*), room temperature; (···) $KCuCl_3$, *ac* face, E‖red (82% *X* and 18% *Y*), 77 K. The energy and reflectivity of the effective transitions used for the transformations were 50 600 cm^{-1} and 18.3%, 51 000 cm^{-1} and 12.6%, 54 000 cm^{-1} and 3.0%, and 51 500 cm^{-1} and 18.3%, respectively.

are also consistent with the coupled-chromophore analysis, as with $KCuCl_3$ there are no additional properties of the ligand field transitions in the dimer that require contributions associated with the binuclear electronic structure.

$LiCuCl_3 \cdot 2H_2O$. Figure 4 shows the low-temperature, molecular-polarized, absorption spectra of $LiCuCl_3 \cdot 2H_2O$. As this binuclear chlorocuprate has no monomeric analogue, only a limited analysis is presented. However, the intensities and polarizations of the ligand field transitions indicate that this complex is similar to the tetragonal binuclear complex $KCuCl_3$ (see Figure 2A, bottom). The additional *Y*-polarized intensity in the higher energy ligand field region is associated with the $a'(d_{xz}) \rightarrow a''(d_{xy})$ transition in C_s symmetry (Table IIB) and reflects some lowering of the single-ion site symmetry in $LiCuCl_3 \cdot 2H_2O$ from C_{2v} (as in $KCuCl_3$) to C_s (as in $((CH_3)_2NH_2)CuCl_3$) due to the differences in axial ligation.

Charge-Transfer Transitions. We have also collected polarized, single-crystal, specular reflectance data on the $KCuCl_3$ {010} crystal faces in the 15 000–45 000-cm^{-1} spectral region (Figure 5A). Figure 5B shows the room-temperature absorption spectra, obtained from Kramers–Kronig transformation of the reflectance spectra, of two crystal polarizations, each with a dominant contribution from different molecular polarizations ((- - -) 82% *X*, 18% *Y*; (-·-) 2% *X*, 5% *Y*, 93% *Z*). The 77 K spectrum of one polarization ((···) 82% *X*, 18% *Y*) is included to indicate the sharpening of these bands upon cooling. Also included, for comparison, is the analogous spectrum of the tetragonal mononuclear complex $(C_2H_5NH_3)_2CuCl_4$ ((—) 48% *XY*, 52% *Z*).

The important observation for this study of the ligand field and dimer transitions is the complete *X* and *Y* polarization of the charge-transfer bands and the lack of *Z*-polarized intensity throughout this spectral region. This absence of *Z*-polarized charge-transfer transitions indicates that lower energy transitions that are predicted to be *Z* polarized in the tetragonal binuclear chlorocuprate will not be able to gain intensity through vibronic coupling or low-symmetry interactions with these Laporte-allowed, charge-transfer transitions. Predicted *Z*-polarized intensity for ligand field transitions is thus not expected to be observed. The charge-transfer spectra of square-planar and tetragonal chlorocuprate monomers have been studied[10] in detail and the two dominant features assigned as the *X*,*Y*-polarized $^2E_u \leftarrow {}^2B_{1g}$ ($4e_u(\pi) \rightarrow 3b_{1g}$) and $^2E_u \leftarrow {}^2B_{1g}$ ($3e_u(\sigma) \rightarrow 3b_{1g}$) transitions. The lack of *Z* intensity in the charge-transfer spectra of the monomer is due to the fact that the only transition predicted to be *Z* polarized, $^2B_{2u} \leftarrow {}^2B_{1g}$ ($1b_{2u}(\pi) \rightarrow 3b_{1g}$), has no overlap of the donor and acceptor orbitals involved in the charge-transfer transition. An analogous explanation is appropriate for the chlorocuprate dimers, as each monomer site still has a $d_{x^2-y^2}$ ground state.[17] However, in a comparison of the *X*,*Y*-polarized monomer and dimer spectra (Figure 5B), the features are clearly different and we are presently involved in a more complete UV spectroscopic study on additional $KCuCl_3$ crystal faces and other Cu dimers to determine the origin of these spectral differences.

Table III

	dimer bands, cm^{-1}		$2J$, cm^{-1}	singlet ϵ_{max}, M^{-1} cm^{-1}, per $Cu_2Cl_6^{2-}$
	major peak	shoulder		
$KCuCl_3$	19 952	21 505	−43	580
$((CH_3)_2NH_2)CuCl_3$	19 091	20 725	−3	374
$LiCuCl_3 \cdot 2H_2O$	20 080	21 622	+68	490

Dimer Transitions. Variable-temperature, polarized, single-crystal absorption spectra have been taken of the dimer transitions of the binuclear chlorocuprates in the 15 000–25 000-cm^{-1} region. Figure 6 shows the low-temperature, molecular-polarized, absorption spectra (Figure 6A) of $KCuCl_3$, $((CH_3)_2NH_2)CuCl_3$, and $LiCuCl_3 \cdot 2H_2O$, the temperature dependence of these spectra (Figure 6B), and plots of integrated dimer band intensity vs. temperature (Figure 6C). Table III lists the energies of the major dimer band and the weak higher energy shoulder[20] of the three complexes.

These transitions of the three binuclear complexes have very similar energies, and their intensities are comparable (vide infra). The polarization of these bands in the two C_{2h} dimers is cleanly along the copper–copper molecular direction (*X*), while in $KCuCl_3$ the band shows a mixed *X*,*Y* polarization. Finally, these three complexes show dramatic differences in the temperature dependence of their dimer band intensities (Figure 6B,C) in the temperature range associated with changes in the population of the ground-state singlet and triplet. Therefore, in contrast to the ligand field region, where the spectral features are those of the single Cu(II) ions perturbed by the dimer structure, these new transitions are a direct consequence of the binuclear electronic structure and their interpretation and assignment requires a correlation to the structural and electronic details of the binuclear complexes. The similarities of these transitions in the three structurally related complexes, however, indicate that the dimer bands have a common assignment.

The polarization of the dimer transition has been reported[4a] to correspond to the copper–copper axis. While our molecular-polarized data clearly show this for the two dimers with C_{2h} symmetry, $((CH_3)_2NH_2)CuCl_3$ and $LiCuCl_3 \cdot 2H_2O$, the major dimer transition in the structurally similar D_{2h} complex $KCuCl_3$ has mixed *X*,*Y* polarization. In D_{2h} *X* and *Y* are, of course, not equivalent, yet both the *X* and *Y*-polarized spectra show similar intensities and a similar temperature dependence. The large difference in polarization of this band between the C_{2h} and D_{2h} dimers indicates that it cannot have a vibronic origin, as this

(20) It should be noted that we observe a second very weak shoulder at 21 164 cm^{-1} in low-temperature $KCuCl_3$ spectra; a similar feature between the major dimer band and the shoulder is also observed in some low-temperature $((CH_3)_2NH_2)CuCl_3$ spectra.

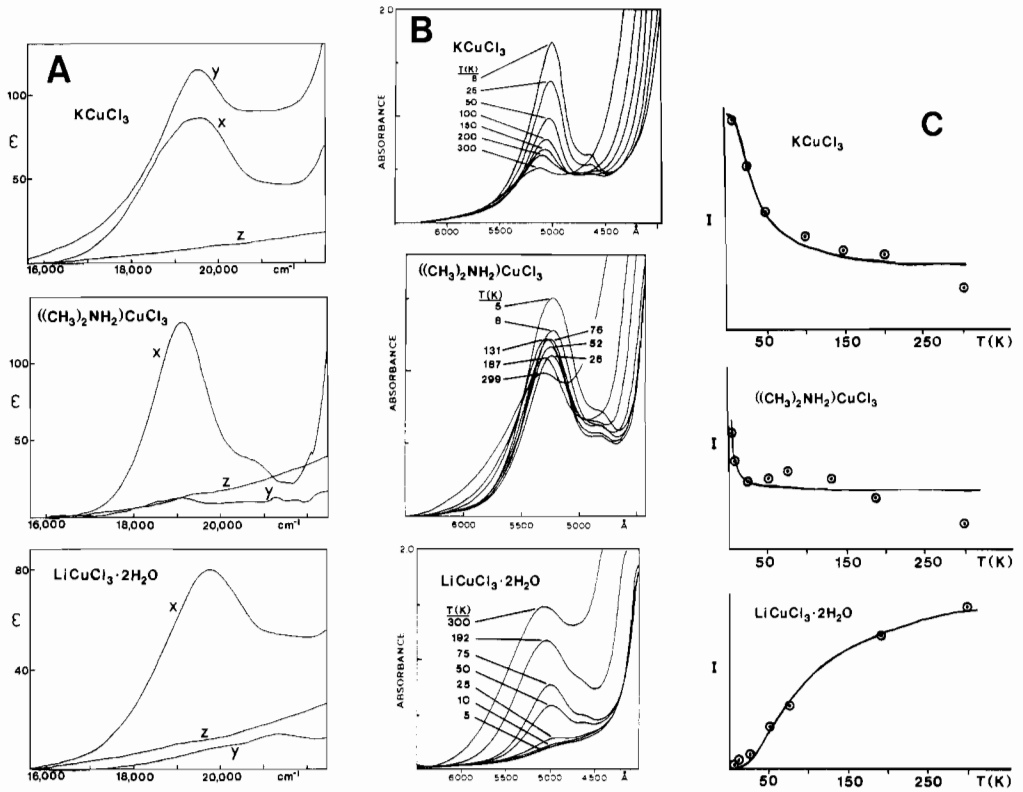

Figure 6. (A) Molecular-polarized absorption spectra (molar extinction values per $Cu_2Cl_6^{2-}$) of the dimer bands: (upper) $KCuCl_3$ (210 K); (middle) $((CH_3)_2NH_2)CuCl_3$ (7 K); (lower) $LiCuCl_3 \cdot 2H_2O$ (192 K). (B) Temperature-dependent spectra: (upper) $KCuCl_3$ (*ac* face E‖yellow; 2% *X*, 5% *Y*, 93% *Z*); (middle) $((CH_3)_2NH_2)CuCl_3$ (*ac* face E‖red; 66% *X*, 33% *Y*, 1% *Z*); (lower) $LiCuCl_3 \cdot 2H_2O$ (*ab* face E‖*a*; 67% *X*, 7% *Y*, 26% *Z*). (C) Plots of the integrated intensity (I) of the dimer bands vs. temperature (the tail of higher energy, more intense transitions has been manually subtracted in determining I). Solid lines are theoretical intensity values determined by a least-squares fit of the experimental points to the Bleaney–Bowers equation (see text) for the population of the singlet ground state.

mechanism should be similar in all three dimers. The mixed polarization for $KCuCl_3$ must therefore derive from a static low-symmetry mixing with intense, allowed, excited states and indicates an effective spectroscopic symmetry lower than D_{2h}. Examination of the $KCuCl_3$ crystal structure[12] shows there to be considerable variation of the Cl_{ax}–Cu–Cl_{eq} angles (80.8–100.6°), which lowers the dimer crystallographic symmetry to C_i. ($((CH_3)_2NH_2)CuCl_3$ and $LiCuCl_3 \cdot 2H_2O$, however, have a clean *X* polarization of these transitions and thus exhibit a spectroscopically effective C_{2h} dimer symmetry.

The dimer transitions show an unusual temperature dependence, which for the case of $KCuCl_3$, where there is a dramatic increase in intensity upon cooling, is inconsistent with a vibronic coupling intensity mechanism. The temperature range of these intensity changes, however, indicates a correlation of the transition intensity to the ground spin state populations. Therefore, we have fit the temperature dependence of the $KCuCl_3$ integrated dimer band intensity (I_i), in the temperature range 7–300 K, to the Bleaney–Bowers relationship[21] for the population of the singlet ground state in an exchange-coupled binuclear $S = {}^1/_2$ system

$$I_i = m/(1 + 3\exp(2J/kT_i))$$

where the isotropic Heisenberg exchange coupling parameter J (based on the Hamiltonian $H = -2JS_1 \cdot S_2$) and the proportionality constant m are adjustable parameters. This fit (solid line in Figure 6C, top) results in an exchange coupling parameter for $KCuCl_3$, $2J = -43$ cm^{-1}, which is very similar to that obtained from magnetic susceptibility measurements[22] ($2J = -37$ cm^{-1}). Therefore, we have analogously fit (see Figure 6C, middle and bottom) the dimer band intensities for the other two complexes, and we list in Table III the exchange coupling parameter $2J$ determined from these fits to the Bleaney–Bowers equation.

The magnetic behavior of the binuclear chlorocuprates, which have structures consisting of chains of stacked $Cu_2Cl_6^{2-}$ dimers (see Figure 1), will of course reflect not only the intradimer properties, but also three-dimensional interdimer magnetic interactions. For $KCuCl_3$, the ground-state magnetic properties are relatively straightforward as the antiferromagnetic exchange coupling[22a] within the planar dimeric unit is the dominant interaction in the single-crystal structure; exchange coupling between copper(II)'s in adjacent dimers of the chain ($2J'$) is only 5–20% of that within the dimer[22b] and interchain interaction is negligible. Thus, experimentally observed magnetic properties of $KCuCl_3$ directly relate to the ground state of the binuclear unit. The situation for the other two binuclear complexes is less clear.

For $((CH_3)_2NH_2)CuCl_3$, which has a nonplanar $Cu_2Cl_6^{2-}$ unit, recent magnetization measurements by Willett[23] indicate that the intradimer exchange interaction is weak and ferromagnetic ($2J = +10$ cm^{-1}) and that the interdimer exchange coupling is antiferromagnetic and is of comparable magnitude ($2J' = -9$ cm^{-1}). The observed magnetic properties of this complex are thus expected to show contributions from both intra- and interdimer effects.

A variety of experimental studies have attempted to elucidate the $LiCuCl_3 \cdot 2H_2O$ ground-state magnetic properties, which, although this salt contains a very similar planar $Cu_2Cl_6^{2-}$ unit, are more complicated than those of $KCuCl_3$. The initial susceptibility data were interpreted[24a] as indicating a ferromagnetic intradimer exchange coupling, and a three-dimensional ordering (paramagnet to antiferromagnet) was observed to occur at low temperature.

(21) Bleaney, B.; Bowers, K. D. *Proc. R. Soc. London, Ser. A.* **1952**, *214*, 451–465.
(22) (a) Maass, G. J.; Gerstein, B. C.; Willett, R. D. *J. Chem. Phys.* **1967**, *46*, 401–402. (b) Hara, K.-I.; Inoue, M.; Emori, S.; Kubo, M. *J. Magn. Reson.* **1971**, *4*, 337–346.
(23) Willett, R. D., private communication.
(24) (a) Vossos, P. H.; Jennings, L. D.; Rundle, R. E. *J. Chem. Phys.* **1960**, *32*, 1590–1591. (b) Forstat, H.; McNeely, D. R. *J. Chem. Phys.* **1961**, *35*, 1594–1596. (c) Metselaar, J. W.; De Klerk, D. *Physica* **1973**, *69*, 499–534. (d) ter Haar, L. W.; Hatfield, W. E. *Inorg. Chem.* **1985**, *24*, 1022–1026.

Table IV. Band Shapes of Mononuclear and Binuclear Chlorocuprate Ligand Field, Dimer, and Charge-Transfer Transitions

	transition[a]	energy, cm^{-1}	fwhm, cm^{-1}	ν_i, cm^{-1}	S_i
	Mononuclear Chlorocuprates				
$(N\text{-mph})_2CuCl_4$[d] (10 K)	$b_{1g}(xy) \rightarrow a_g(x^2-y^2)$	12 500	1250	276	3.7
	$b_{3g}(yz) \rightarrow a_g(x^2-y^2)$	14 050	1400	276	4.6
	$a_g(z^2) \rightarrow a_g(x^2-y^2)$	17 000	1500	276	5.3
$(metH)_2CuCl_4$ (7 K)	$a_{1g}(nb) \rightarrow b_{2g}$[b]	22 320	1250	276	3.7
	Binuclear Chlorocuprate				
$KCuCl_3$ (Y polarizn) (7 K)	$a_1(z^2) \rightarrow b_2(xy)$	10 650	1360	278	4.3[e]
	$a_1(x^2-y^2) \rightarrow b_2(xy)$	11 910	1260	278	3.7
	$b_1(xz), a_2(yz) \rightarrow b_2(xy)$	13 150	1400	278	4.6
$KCuCl_3$ (8 K)		19 950[c]	1360	278	4.3

[a] All are ligand field transitions unless otherwise noted. [b] Charge-transfer transition. [c] Dimer band. [d] Data from ref 9a. [e] Obtained from the mononuclear S_i values by adjusting the energies and intensities of the analogous $(N\text{-mph})_2CuCl_4$ transitions to fit the $KCuCl_3$ ligand field envelope and then allowing the band shapes to vary to improve the fit (see Figure 2B, bottom).

However, heat capacity data at this transition temperature (4.4 K) indicated[24b] a system of $S = {}^1/_2$ ions and not $S = 1$ dimers above this Néel temperature. Phase transitions observed in single-crystal, variable-field, susceptibility experiments have been interpreted[24c] as indicating four different exchange interactions in the −15 to +15 cm^{-1} range, with a ferromagnetic intradimer interaction ($2J = +15$ cm^{-1}) and an antiferromagnetic coupling of similar magnitude ($2J' = -15$ cm^{-1}) between copper(II)'s on adjacent dimers. Recently, ter Haar and Hatfield[24d] fit their powder susceptibility data on $LiCuCl_3 \cdot 2H_2O$ to an alternating Heisenberg linear-chain model and obtained $2J = -7.4$ cm^{-1}, with an alternation parameter ($\alpha = 0.89$) indicating about 90% linear uniform chain behavior of $S = {}^1/_2$ ions. Magneto–structural correlations that have been empirically and theoretically developed[2,3] for binuclear Cu(II) complexes would argue that a weakly antiferromagnetic intradimer interaction should be observed for the planar $Cu_2Cl_6^{2-}$ unit in $LiCuCl_3 \cdot 2H_2O$, similar to that found in $KCuCl_3$. However, interdimer (intrachain) and interchain interactions in the single-crystal structure of this complex appear to have a major effect on the observed magnetic properties.

For $KCuCl_3$, which has a dominant intradimer exchange coupling, we find a good correlation between the sign and magnitude of the ground-state singlet–triplet splitting determined by magnetic susceptibility measurements[22] and the sign and magnitude of $2J$ we obtain by fitting the intensity of the dimer transition to the population of the singlet ground state. Since the intensity of the dimer band thus depends only on the population of the singlet ground state, this spectral feature can be assigned as a spin-allowed, singlet-to-singlet transition of the binuclear chlorocuprate electronic structure. The similarity of the dimer bands among the three salts requires an analogous assignment in each case.

For $((CH_3)_2NH_2)CuCl_3$, the temperature dependence of the dimer band intensity in the 5–300 K range is complex, showing (Figure 6B,C, middle) an increase, a decrease, and a further increase upon cooling. Fitting this data to the Bleaney–Bowers equation gives an exchange coupling parameter of $2J = -3$ cm^{-1}; however, in contrast to $KCuCl_3$ the fit is poor (see Figure 6C). It therefore appears that the weak magnetic interactions within the three-dimensional structure are affecting the net dimer magnetic ground state and thus the intensity of the dimer transition in $((CH_3)_2NH_2)CuCl_3$.

The temperature dependence of the $LiCuCl_3 \cdot 2H_2O$ dimer band is clear and dramatic, with essentially all intensity lost upon cooling to 5 K (Figure 6B, bottom). A fit of this intensity to the Bleaney–Bowers relationship[25] indicates a dominant ferromagnetic interaction ($2J = +68$ cm^{-1}) within the dimer ground state at temperatures above the phase transition (4.4 K). Thus, there is an interesting difference between the ground-state magnetic interaction of the $LiCuCl_3 \cdot 2H_2O$ dimer site as indicated by the temperature dependence of the dimer band intensity (clear ferromagnetism) and as indicated by recent bulk magnetic susceptibility measurements (weak antiferromagnetism); this discrepancy warrants further investigation of this complex.

On the basis of the above assignment of the dimer band as an allowed singlet-to-singlet excitation, the maximum molar extinction coefficients (per $Cu_2Cl_6^{2-}$ structural unit) for this transition in the three dimers have been determined by using the isotropic $2J$ values and extrapolating to 100% population of the singlet component of the ground state. These values are indicated in Table III and show that although the polarizations vary, all three dimer bands have total intensities of similar magnitude.

A major advantage to studying the binuclear chlorocuprates is the separation of the dimer transitions from other electronic features, allowing a clear evaluation of the entire dimer band shape. The Franck–Condon factors that dictate the band shape of a transition are quantified by the Huang–Rhys parameters S_i ($S_i = E_i/\nu_i$, where E_i is the lowering of the energy of the excited state in the normal mode Q_i due to an excited-state distortion), which can be determined[26] through a second-moment (m_2) analysis of the band, based on an effective vibrational frequency (ν_i):

$$m_2 = S_i \nu_i^2 \coth (\nu_i/2kT)$$

For Gaussian bands, the second moment is also related to the full bandwidth at half-maximum (fwhm):

$$m_2 = (\text{fwhm})^2/8 \ln 2$$

These two relationships thus allow a straightforward determination of the Huang–Rhys parameters from the experimental bands. Table IV gives the results of a low-temperature band-shape analysis of (1) the well-resolved and vibrationally structured ligand field transitions of the square-planar monomer bis(methylphenethylammonium) tetrachlorocuprate(II) ($(N\text{-mph})_2CuCl_4$; data from ref 9a), (2) the well-resolved, lowest energy, nonbonding, $a_{2g} \rightarrow b_{1g}$ charge-transfer transition of the square-planar monomer dimethadonium tetrachlorocuprate(II) ($(metH)_2CuCl_4$), (3) the Gaussian-resolved ligand field transitions (Y-polarized spectrum) of $KCuCl_3$ (see Figure 2B, lower), and (4) the dimer band of $KCuCl_3$ (see Figure 6B, top); effective vibrational frequencies (ν_i) for the ground state totally symmetric breathing mode of 276 cm^{-1} for the mononuclear[9a] complexes and 278 cm^{-1} for $KCuCl_3$[27] were used in this analysis. The Huang–Rhys parameters estimated from this second-moment analysis of the structured ligand field transitions of $(N\text{-mph})_2CuCl_4$ are in reasonable agreement with those obtained from a fit to the progressional intensity distribution.[26] These band shapes will be considered below in light of possible assignments of the dimer transitions.

Discussion

The above analysis of the spectral data on the ligand field transitions of the mononuclear and binuclear chlorocuprates clearly

(25) Fitting this data set to a vibronic mechanism results in an unrealistic effective vibrational frequency of 8 cm^{-1}.

(26) Solomon, E. I. *Comments Inorg. Chem.* **1984**, *5*, 225–320.
(27) Adams, D. M.; Lock, P. J. *J. Chem. Soc. A* **1967**, 620–623.

Table V. Coupled-Chromophore Analysis for Simultaneous Pair Excitations and $Cu(II)_A \rightarrow Cu(II)_B$ Charge-Transfer Transitions[a]

A. Tetragonal $Cu_2Cl_6^{2-}$

	single-ion transitions[b]	excited states[c]	polarizn
	Double Excitations (SPE's)		
$(z^2 \rightarrow xy) \times 2$	$(a_1 \rightarrow b_2) \times 2$	^1A_g, $^3B_{3u}$	
$(x^2 - y^2 \rightarrow xy) \times 2$	$(a_1 \rightarrow b_2) \times 2$	^1A_g, $^3B_{3u}$	
$(xz \rightarrow xy) \times 2$	$(b_1 \rightarrow b_2) \times 2$	^1A_g, $^3B_{3u}$	
$(yz \rightarrow xy) \times 2$	$(a_2 \rightarrow b_2) \times 2$	^1A_g, $^3B_{3u}$	
$(z^2 \rightarrow xy) + (x^2 - y^2 \rightarrow xy)$	$(a_1 \rightarrow b_2) + (a_1 \rightarrow b_2)$	^1A_g, $^1B_{3u}$, ^3A_g, $^3B_{3u}$	x
$(z^2 \rightarrow xy) + (xz \rightarrow xy)$	$(a_1 \rightarrow b_2) + (b_1 \rightarrow b_2)$	$^1B_{2g}$, $^1B_{1u}$, $^3B_{2g}$, $^3B_{1u}$	z
$(z^2 \rightarrow xy) + (yz \rightarrow xy)$	$(a_1 \rightarrow b_2) + (a_2 \rightarrow b_2)$	$^1B_{3g}$, ^1A_u, $^3B_{3g}$, ^3A_u	
$(x^2 - y^2 \rightarrow xy) + (xz \rightarrow xy)$	$(a_1 \rightarrow b_2) + (b_1 \rightarrow b_2)$	$^1B_{2g}$, $^1B_{1u}$, $^3B_{2g}$, $^3B_{1u}$	z
$(x^2 - y^2 \rightarrow xy) + (yz \rightarrow xy)$	$(a_1 \rightarrow b_2) + (a_2 \rightarrow b_2)$	$^1B_{3g}$, ^1A_u, $^3B_{3g}$, ^3A_u	
$(xz \rightarrow xy) + (yz \rightarrow xy)$	$(b_1 \rightarrow b_2) + (a_2 \rightarrow b_2)$	$^1B_{1g}$, $^1B_{2u}$, $^3B_{1g}$, $^3B_{2u}$	y
	Charge-Transfer Transitions ($Cu(II)_A \rightarrow Cu(II)_B$)		
$xy \rightarrow xy$	$b_2 \rightarrow b_2$	^1A_g, $^1B_{3u}$	x
$z^2 \rightarrow xy$	$a_1 \rightarrow b_2$	$^1B_{1g}$, $^1B_{2u}$, $^3B_{1g}$, $^3B_{2u}$	y
$x^2 - y^2 \rightarrow xy$	$a_1 \rightarrow b_2$	$^1B_{1g}$, $^1B_{2u}$, $^3B_{1g}$, $^3B_{2u}$	y
$xz \rightarrow xy$	$b_1 \rightarrow b_2$	$^1B_{3g}$, ^1A_u, $^3B_{3g}$, ^3A_u	
$yz \rightarrow xy$	$a_2 \rightarrow b_2$	$^1B_{2g}$, $^1B_{1u}$, $^3B_{2g}$, $^3B_{1u}$	z

B. Square-Pyramidal $Cu_2Cl_6^{2-}$

	single-ion transitions[d]	excited states[e]	polarizn
	Double Excitations (SPE's)		
$(z^2 \rightarrow xy) \times 2$	$(a' \rightarrow a'') \times 2$	^1A_g, ^3B_u	
$(x^2 - y^2 \rightarrow xy) \times 2$	$(a' \rightarrow a'') \times 2$	^1A_g, ^3B_u	
$(xz \rightarrow xy) \times 2$	$(a' \rightarrow a'') \times 2$	^1A_g, ^3B_u	
$(yz \rightarrow xy) \times 2$	$(a'' \rightarrow a'') \times 2$	^1A_g, ^3B_u	
$(z^2 \rightarrow xy) + (x^2 - y^2 \rightarrow xy)$	$(a' \rightarrow a'') + (a' \rightarrow a'')$	^1A_g, ^1B_u, ^3A_g, ^3B_u	x,z
$(z^2 \rightarrow xy) + (xz \rightarrow xy)$	$(a' \rightarrow a'') + (a' \rightarrow a'')$	^1A_g, ^1B_u, ^3A_g, ^3B_u	x,z
$(z^2 \rightarrow xy) + (yz \rightarrow xy)$	$(a' \rightarrow a'') + (a'' \rightarrow a'')$	^1B_g, ^1A_u, ^3B_g, ^3A_u	y
$(x^2 - y^2 \rightarrow xy) + (xz \rightarrow xy)$	$(a' \rightarrow a'') + (a' \rightarrow a'')$	^1A_g, ^1B_u, ^3A_g, ^3B_u	x,z
$(x^2 - y^2 \rightarrow xy) + (yz \rightarrow xy)$	$(a' \rightarrow a'') + (a'' \rightarrow a'')$	^1B_g, ^1A_u, ^3B_g, ^3A_u	y
$(xz \rightarrow xy) + (yz \rightarrow xy)$	$(a' \rightarrow a'') + (a'' \rightarrow a'')$	^1B_g, ^1A_u, ^3B_g, ^3A_u	y
	Charge-Transfer Transitions ($Cu(II)_A \rightarrow Cu(II)_B$)		
$xy \rightarrow xy$	$a'' \rightarrow a''$	^1A_g, ^1B_u	x,z
$z^2 \rightarrow xy$	$a' \rightarrow a''$	^1B_g, ^1A_u, ^3B_g, ^3A_u	y
$x^2 - y^2 \rightarrow xy$	$a' \rightarrow a''$	^1B_g, ^1A_u, ^3B_g, ^3A_u	y
$xz \rightarrow xy$	$a' \rightarrow a''$	^1B_g, ^1A_u, ^3B_g, ^3A_u	y
$yz \rightarrow xy$	$a'' \rightarrow a''$	^1A_g, ^1B_u, ^3A_g, ^3B_u	x,z

[a] Approximate order of ascending energy is based on single-ion ligand field transition assignments. [b] C_{2v} monomer: $^2B_2(d_{xy})$ ground state. [c] D_{2h} dimer: ^1A_g, $^3B_{3u}$ ground state. [d] C_s monomer: $^2A''(d_{xy})$ ground state. [e] C_{2h} dimer: ^1A_g, ^3B_u ground state.

indicates that the d–d transitions are not significantly perturbed by the binuclear electronic structure. The observed increase in ligand field transition intensity is found to arise from the lower symmetry of the two Cu(II) ion sites within the dimer structure; specific single-ion d–d transitions become electric-dipole-allowed and therefore more intense in this noncentrosymmetric site geometry. The remainder of the discussion, therefore, will focus on the spectral properties of the chlorocuprate dimer bands in order to experimentally assign these spectral features of the binuclear Cu(II) electronic structure.

There are two reasonable assignments for the dimer bands, which, from the temperature dependence of their intensity (see Figure 6B), are clearly observed to be singlet-to-singlet transitions of the binuclear chlorocuprates. They could be simultaneous pair excitations[28] (SPE), which correspond to a one-photon excitation of a ligand field transition on both Cu(II) centers, made allowed by the exchange interaction. Alternatively, they could be ligand-to-metal charge-transfer transitions, which are found at considerably lower energy in the binuclear structure relative to those of the monomer. These two possible assignments are now examined with respect to the data.

Simultaneous Pair Transition. Assignment of the dimer transitions as simultaneous pair excitations can be evaluated within the coupled chromophore model.[7b] Table V gives all possible symmetric and antisymmetric combinations of single-ion transitions, the dimer ground states and excited states, and the polarizations of the spin-allowed, parity-allowed, double excitations (SPE's) for the D_{2h} (Table VA) and C_{2h} (Table VB) dimer symmetries. In this table the double excitations are ordered in approximately ascending energy on the basis of the sum of the experimental energies of the contributing single-ion ligand field transitions. Also indicated in Table V are the copper(II)-to-copper(II) charge-transfer transitions of the binuclear complex, the dimer excited states formed from these transitions, and the polarizations of these transitions, which are spin- and parity-allowed in the dimer symmetries. We first consider the square-pyramidal C_{2h} dimers $((CH_3)_2NH_2)CuCl_3$ and $LiCuCl_3{\cdot}2H_2O$, which have a cleanly X-polarized dimer band. The large difference in polarization between these dimer bands and that of $KCuCl_3$ indicates that their intensity cannot be due to a vibronic mechanism but must relate to an electric-dipole-allowed transition in the appropriate effective site symmetry. The lowest energy X,Z-polarized pair transition (Table VB) corresponds to the sum of the $d_{z^2} \rightarrow d_{xy}$ transition on one copper(II) and the $d_{x^2-y^2} \rightarrow d_{xy}$ transition on the second copper(II). Considering both the singlet and triplet components of the ground state, this transition gives rise to four spin-allowed dimer electronic transitions: a parity-allowed singlet ($^1B_u \leftarrow {}^1A_g$), a parity-allowed triplet ($^3A_g \leftarrow {}^3B_u$), a parity-forbidden singlet ($^1A_g \leftarrow {}^1A_g$), and a parity-forbidden triplet ($^3B_u \leftarrow {}^3B_u$). For the D_{2h} complex $KCuCl_3$ (Table VA) the analogous pair transition is comprised of a parity-allowed, X-polarized singlet ($^1B_{3u} \leftarrow {}^1A_g$) and triplet ($^3A_g \leftarrow {}^3B_{3u}$) and a parity-forbidden singlet ($^1A_g \leftarrow {}^1A_g$) and triplet ($^3B_{3u} \leftarrow {}^3B_{3u}$); the mixed X,Y polarization of the $KCuCl_3$ dimer band thus re-

(28) (a) Varsanyi, F.; Dieke, G. H. *Phys. Rev. Lett.* **1961**, *7*, 442–443. (b) Dexter, D. L. *Phys. Rev.* **1962**, *126*, 1962–1967.

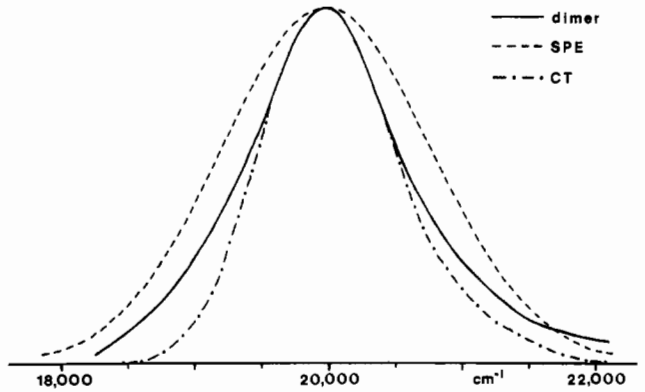

Figure 7. (—) Superposition of the $KCuCl_3$ dimer band absorption spectrum (underlying tail of the intense charge-transfer transitions and the higher energy shoulder have been manually subtracted; *ac* face, E‖yellow (2% *X*, 5% *Y*, 93% *Z*); 8 K) (---) predicted 7 K Gaussian SPE band from the assignment in the text; (-·-) $^2A_{2g} \leftarrow {}^2B_{1g}$ ($1a_{2g}(nb) \rightarrow 3b_{1g}$) charge-transfer transition of dimethadonium tetrachlorocuprate (underlying shoulder of the intense charge-transfer transitions has been manually subtracted; *a*b* face, E‖*a** (17% *X*, 77% *Y*, 6% *Z*); 7 K).

quires a lower effective dimer symmetry ($D_{2h} \rightarrow C_i$; vide supra) in this complex.

In an earlier detailed spectroscopic study[29] of Yb_2O_3, weak electronic transitions were assigned as simultaneous pair excitations primarily on the basis of their band shapes. The experiments and theory developed in that study showed that the band shape of a SPE depends on the product of the squares of the vibrational overlap integrals of the two independent ligand field excitations and therefore on the *sum* of the Huang–Rhys parameters of the two single-ion excitations, providing the vibrational frequencies are similar; i.e.

$$S_{SPE} = S_{(d\rightarrow d)A} + S_{(d\rightarrow d)B}$$

where $S_{(d\rightarrow d)A}$ is the Huang–Rhys parameter of a ligand field transition on Cu_A, etc. This correlation between the band shape of the SPE and the band shapes of the single-ion transitions is required for assignment of the chlorocuprate dimer bands as simultaneous pair excitations. Table IV compares the band shapes of the single-ion ligand field transitions and the $KCuCl_3$ dimer transition. The Huang–Rhys parameter of the $KCuCl_3$ dimer band (4.3), however, is found to be of magnitude similar to those of the single-ion ligand field transitions (~4) and approximately half of the expected sum (8.0 = 4.3 ($z^2 \rightarrow xy$) + 3.7 ($x^2 - y^2 \rightarrow xy$)) of the two ligand field values. This point is clearly illustrated in Figure 7, which shows a superposition of the $KCuCl_3$ dimer band and the predicted Gaussian SPE band shape based on the sum of the Huang–Rhys parameters of the $d_{z^2} \rightarrow d_{xy}$ and $d_{x^2-y^2} \rightarrow d_{xy}$ ligand field transitions from the above SPE assignment. The band shape of the dimer transition is observed to be too sharp relative to that predicted for a simultaneous pair excitation of this complex; this strongly argues against the SPE assignment.

Further, based on the single-ion transition energies from the Gaussian resolved ligand field bands, the dimer band in $KCuCl_3$ is 2600 cm^{-1} lower in energy than that predicted from the above assignment as the lowest energy SPE ($E_{SPE} = E_{z^2\rightarrow xy} + E_{x^2-y^2\rightarrow xy}$ = 22 550 cm^{-1} compared to E_{dimer} = 19 950 cm^{-1}; see Table I). Although the energies of SPE's may not be exactly additive, the largest experimentally observed deviation for an SPE transition was 370 cm^{-1} higher in energy than predicted; this large deviation for the $^4T_{1g}(G) + {}^4T_{1g}(G)$ transition in $RbMnF_3$ has been explained[30] as arising from strong exciton–lattice coupling between two highly distorted excited states. Thus, the experimental energy of the dimer band in $KCuCl_3$ is not consistent with the SPE assignment.

Table VI. Correlation of One-Electron Molecular Orbitals of D_{4h} $CuCl_4^{2-}$ and D_{2h} and C_{2h} $Cu_2Cl_6^{2-}$

	mononuclear	binuclear	
	D_{4h}	D_{2h}	C_{2h}
Cu 3d	b_{2g} (xy) (gs)	b_{1g},b_{2u} (gs)	b_g,a_u (gs)
	a_{1g} (z^2)	a_g,b_{3u}	a_g,b_u
	b_{1g} ($x^2 - y^2$)	a_g,b_{3u}	a_g,b_u
	e_g (xz,yz)	b_{2g},b_{1u} / b_{3g},a_u	a_g,b_u / b_g,a_u
Cl^- pπ (in plane)	a_{2g}	b_{1g}	b_g
	e_u	b_{2u} / b_{3u}	a_u / b_u
Cl^- pπ (out of plane)	b_{1g}	a_g	a_g
	b_{1u}	a_u	a_u
	a_{2u}	b_{1u},[a] b_{1u}[b]	b_u,[a] b_u[b]
	e_g	b_{2g},[a] b_{3g}[b] / b_{3g}	a_g,[a] b_g[b] / b_g
Cl^- pσ	e_u	b_{2u},[a] b_{2u}[b] / b_{3u},[a] b_{3u}[b]	a_u,[a] a_u[b] / b_u,[a] b_u[b]
	b_{2g}	b_{1g},[a] b_{1g}[b]	b_g,[a] b_g[b]
	a_{1g}	a_g,[a] a_g[b]	a_g,[a] a_g[b]

[a] Terminal. [b] Bridging.

Finally, the dimer bands have been found to be parity-allowed singlet-to-singlet transitions; therefore, in the SPE assignment the corresponding parity-allowed triplet pair transitions would either have to be significantly higher in energy (>3000 cm^{-1}) and obscured by the more intense charge-transfer transitions or would have to lack an intensity mechanism available to the singlet transitions. The former possibility would correspond to an antiferromagnetic-type stabilization of the singlet SPE excited state relative to the corresponding triplet SPE and would, in fact, explain the observation (vide supra) that the singlet dimer band is 2600 cm^{-1} lower than the sum of the single-ion d → d transition energies. However, this explanation would require a very large exchange coupling in this SPE excited state, which is not reasonable since it would involve coupling a hole in the d_{z^2} orbital on one Cu(II) to a hole in the $d_{x^2-y^2}$ orbital on the adjacent Cu(II) at a 3.4-Å distance in the dimer. With respect to the alternative possibility of a unique singlet intensity mechanism, simultaneous pair excitations are formally two-electron excitations and, therefore, they must gain intensity from mixing with intense, higher energy, one-electron transitions. The one source of intensity in the dimer that would contribute only to singlet transitions involves mixing with the $Cu^{II}(d_{xy}) \rightarrow Cu^{II}(d_{xy})$ charge-transfer transition. If the spin- and parity-allowed ($d_{z^2} \rightarrow d_{xy}$) + ($d_{x^2-y^2} \rightarrow d_{xy}$) SPE ($^1B_{3u} \leftarrow {}^1A_g$ and $^3A_g \leftarrow {}^3B_{3u}$ in D_{2h} (see Table VA) and $^1B_u \leftarrow {}^1A_g$ and $^3A_g \leftarrow {}^3B_u$ in C_{2h} (see Table VB)) obtains its intensity through configurational interaction with this lowest energy Cu(II)-to-Cu(II) transition ($^1B_{3u} \leftarrow {}^1A_g$ in D_{2h} (see Table VA) and $^1B_u \leftarrow {}^1A_g$ in C_{2h} (see Table VB)), only the singlet SPE transition can gain intensity, as is observed. This Cu(II) → Cu(II) charge-transfer intensity mechanism would then explain the *X* polarization of the singlet dimer bands, since the singlet-only Cu(II)-to-Cu(II) transition is predicted to have *X*-polarized intensity. This intensity mechanism, however, would not account for the somewhat larger *Y*-polarization intensity observed in the singlet dimer transition of $KCuCl_3$ without an unreasonably large C_i site distortion of the Cu(II)'s in the *Y* direction. Further, this Cu(II) → Cu(II) charge-transfer intensity mechanism would predict that, for the C_{2h} dimers, particularly the square-pyramidal dimer $((CH_3)_2N\text{-}H_2)CuCl_3$, the dimer band should gain some *Z*-polarized singlet intensity from configurational interaction mixing and this is not observed.

Thus, the band shape, energy, and singlet polarization mechanism all argue strongly against an SPE assignment of the dimer band.

Charge-Transfer Transition. The alternative assignment of the dimer bands would be chloride-to-copper(II) charge-transfer excitations, which are at significantly lower energy in the binuclear structure than in the monomer. Table VI gives the symmetries

(29) Schugar, H. J.; Solomon, E. I.; Cleveland, W. L.; Goodman, L. *J. Am. Chem. Soc.* **1975**, *97*, 6442–6450.
(30) (a) Stokowski, S. E.; Sell, D. D.; Guggenheim, H. J. *Phys. Rev. B: Solid State* **1971**, *4* (9), 3141–3152. (b) Fujiwara, T. *J. Phys. Soc. Jpn.* **1973**, *34*, 36–43.

Table VII. One-Electron Charge-Transfer Transitions for D_{4h} $CuCl_4^{2-}$ and D_{2h} and C_{2h} $Cu_2Cl_6^{2-}$: Final Hole Configurations, Excited States, and Spin-Allowed Polarizations

A. D_{4h} $CuCl_4^{2-}$

Ground State $^2B_{2g}$

final hole config	excited state	polarizn	final hole config	excited state	polarizn	final hole config	excited state	polarizn
a_{2g}	$^2A_{2g}$		b_{1u}	$^2B_{1u}$		e_u	^2E_u	
e_u	^2E_u	x,y	a_{2u}	$^2A_{2u}$	z	b_{2g}	$^2B_{2g}$	x,y
b_{1g}	$^2B_{1g}$		e_g	^2E_g		a_{1g}	$^2A_{1g}$	

B. D_{2h} $Cu_2Cl_6^{2-}$

ligand orbital	ground state	excited state	ground state
$1/2^{1/2}\{\|a^+a^-\| - \|b^+b^-\|\}$	^1A_g	$\|a^+b^+\|$	$^3B_{3u}$

ligand orbital	final 2-hole config[b] (ligand,metal)	excited state	spin-allowed polarizn	ligand orbital	final 2-hole config[b] (ligand,metal)	excited state	spin-allowed polarizn
			pπ In-Plane (Terminal Only)				
b_{1g}	b_{1g},b_{2u}	$^{1,3}B_{3u}$	singlet x	b_{3u}	b_{3u},b_{2u}	$^{1,3}B_{1g}$	triplet y
	b_{1g},b_{1g}	$^{1,3}A_g$	triplet x		b_{3u},b_{1g}	$^{1,3}B_{2u}$	singlet y
b_{2u}	b_{2u},b_{2u}	$^{1,3}A_g$	triplet x	a_g	a_g,b_{2u}	$^{1,3}B_{2u}$	singlet y
	b_{2u},b_{1g}	$^{1,3}B_{3u}$	singlet x		a_g,b_{1g}	$^{1,3}B_{1g}$	triplet y
			pπ Out-of-Plane				
a_u (terminal)	a_u,b_{2u}	$^{1,3}B_{2g}$	triplet z	b_{2g} (terminal)	b_{2g},b_{2u}	$^{1,3}A_u$	
	a_u,b_{1g}	$^{1,3}B_{1u}$	singlet z		b_{2g},b_{1g}	$^{1,3}B_{3g}$	
b_{1u} (terminal)	b_{1u},b_{2u}	$^{1,3}B_{3g}$		b_{3g} (terminal)	b_{3g},b_{2u}	$^{1,3}B_{1u}$	singlet z
	b_{1u},b_{1g}	$^{1,3}A_u$			b_{3g},b_{1g}	$^{1,3}B_{2g}$	triplet z
b_{1u} (bridging)	b_{1u},b_{2u}	$^{1,3}B_{3g}$		b_{3g} (bridging)	b_{3g},b_{2u}	$^{1,3}B_{1u}$	singlet z
	b_{1u},b_{1g}	$^{1,3}A_u$			b_{3g},b_{1g}	$^{1,3}B_{2g}$	triplet z
			pσ (Terminal and Bridging)				
b_{2u}	b_{2u},b_{2u}	$^{1,3}A_g$	triplet x	b_{1g}	b_{1g},b_{2u}	$^{1,3}B_{3u}$	singlet x
	b_{2u},b_{1g}	$^{1,3}B_{3u}$	singlet x		b_{1g},b_{1g}	$^{1,3}A_g$	triplet x
b_{3u}	b_{3u},b_{2u}	$^{1,3}B_{1g}$	triplet y	a_g	a_g,b_{2u}	$^{1,3}B_{2u}$	singlet y
	b_{3u},b_{1g}	$^{1,3}B_{2u}$	singlet y		a_g,b_{1g}	$^{1,3}B_{1g}$	triplet y

	determinantal wave function[a]	excited state		determinantal wave function[a]	excited state	spin-allowed polarizn
$Cu^{II}(d_{xy}) \rightarrow Cu^{II}(d_{xy})$	$1/2^{1/2}\{\|a^+a^-\| + \|b^+b^-\|\}$	^1A_u	$Cu^{II}(d_{xy}) \rightarrow Cu^{II}(d_{xy})$	$1/2^{1/2}\{\|a^+b^-\| + \|a^-b^+\|\}$	$^1B_{3u}$	singlet x

C. C_{2h} $Cu_2Cl_6^{2-}$

	determinantal wave function[a]	ground state		determinantal wave function[a]	ground state
	$1/2^{1/2}\{\|a^+a^-\| - \|b^+b^-\|\}$	^1A_g		$\|a^+b^+\|$	^3B_u

ligand orbital	final 2-hole config[b] (ligand,metal)	excited state	spin-allowed polarizn	ligand orbital	final 2-hole config[b] (ligand,metal)	excited state	spin-allowed polarizn
			pπ In-Plane (Terminal Only)				
b_g	b_g,a_u	$^{1,3}B_u$	singlet x,z	b_u	b_u,a_u	$^{1,3}B_g$	triplet y
	b_g,b_g	$^{1,3}A_g$	triplet x,z		b_u,b_g	$^{1,3}A_u$	singlet y
a_u	a_u,a_u	$^{1,3}A_g$	triplet x,z	a_g	a_g,a_u	$^{1,3}A_u$	singlet y
	a_u,b_g	$^{1,3}B_u$	singlet x,z		a_g,b_g	$^{1,3}B_g$	triplet y
			pπ Out-of-Plane				
a_u (terminal)	a_u,a_u	$^{1,3}A_g$	triplet x,z	a_g (terminal)	a_g,a_u	$^{1,3}A_u$	singlet y
	a_u,b_g	$^{1,3}B_u$	singlet x,z		a_g,b_g	$^{1,3}B_g$	triplet y
b_u (terminal)	b_u,a_u	$^{1,3}B_g$	triplet y	b_g (terminal)	b_g,a_u	$^{1,3}B_u$	singlet x,z
	b_u,b_g	$^{1,3}A_u$	singlet y		b_g,b_g	$^{1,3}A_g$	triplet x,z
b_u (bridging)	b_u,a_u	$^{1,3}B_g$	triplet y	b_g (bridging)	b_g,a_u	$^{1,3}B_u$	singlet x,z
	b_u,b_g	$^{1,3}A_u$	singlet y		b_g,b_g	$^{1,3}A_g$	triplet x,z
			pσ (Terminal and Bridging)				
a_u	a_u,a_u	$^{1,3}A_g$	triplet x,z	b_g	b_g,a_u	$^{1,3}B_u$	singlet x,z
	a_u,b_g	$^{1,3}B_u$	singlet x,z		b_g,b_g	$^{1,3}A_g$	triplet x,z
b_u	b_u,a_u	$^{1,3}B_g$	triplet y	a_g	a_g,a_u	$^{1,3}A_u$	singlet y
	b_u,b_g	$^{1,3}A_u$	singlet y		a_g,b_g	$^{1,3}B_g$	triplet y

	determinantal wave function[a]	excited state	spin-allowed polarizn		determinantal wave function[a]	excited state	spin-allowed polarizn
$Cu^{II}(d_{xy}) \rightarrow Cu^{II}(d_{xy})$	$1/2^{1/2}\{\|a^+a^-\| + \|b^+b^-\|\}$	^1A_u	singlet y	$Cu^{II}(d_{xy}) \rightarrow Cu^{II}(d_{xy})$	$1/2^{1/2}\{\|a^+b^-\| + \|a^-b^+\|\}$	^1B_u	singlet x,z

Table VII (Continued)

[a] Determinantal wave functions are given for configurations of the half-filled valence d_{xy} Cu(II) orbitals where

$$a = 1/2^{1/2}\{d_{xy}(Cu_A) + d_{xy}(Cu_B)\}$$

$$b = 1/2^{1/2}\{d_{xy}(Cu_A) - d_{xy}(Cu_B)\}$$

[b] Each final two-hole configuration (ligand,metal) corresponds to the determinantal wave functions

$$^3\Gamma = |\text{ligand}^+,\text{metal}^+| \qquad ^1\Gamma = 1/2^{1/2}(|\text{ligand}^+,\text{metal}^-| - |\text{ligand}^-,\text{metal}^+|)$$

of the one-electron molecular orbitals for the D_{4h} tetragonal mononuclear complex and the correlations to the D_{2h} and C_{2h} $Cu_2Cl_6^{2-}$ binuclear structures. Also included in Table VI are the additional molecular orbitals contributed by the bridging Cl^-'s in the dimers. Table VII then gives the ground and excited states associated with all the possible one-electron, charge-transfer transitions from these chloride molecular orbitals to the metal-centered, half-occupied, molecular orbitals in these complexes. Note that four states are associated with each Cl → Cu charge transfer in the dimers (Table VIIB,C) as the hole on the metal in the final two-hole configuration can occupy either the $b_{1g} = 1/2^{1/2}[d_{xy}(A) + d_{xy}(B)]$ or $b_{2u} = 1/2^{1/2}[d_{xy}(A) - d_{xy}(B)]$ molecular orbital and each generates both a singlet and triplet final state. Also included in Table VIIB,C are the excited states associated with the lowest energy, singlet-only, Cu(II)-to-Cu(II) ($d_{xy} \rightarrow d_{xy}$) charge-transfer transition in the molecular orbital formalism and the associated electric dipole selection rules for all the transitions.

We first consider the cleanly X-polarized dimer bands of the C_{2h} complexes. A charge-transfer assignment for the dimer band requires a transition originating from a low-energy, nonbonding, chloride, π molecular orbital, which in C_{2h} symmetry gives rise to X,Z-polarized transitions. The X intensity will come from configurational interaction with intense charge-transfer bands, while Z intensity is not observed due to the lack of overlap between the π donor and d_{xy} acceptor orbitals involved in the charge-transfer process (vide supra). There are five chloride π molecular orbitals giving rise to $^1B_u \leftarrow {}^1A_g$ X,Z-polarized transitions (see Table VIIC): two terminal in-plane (nonbonding) molecular orbitals b_g and a_u, two terminal out-of-plane molecular orbitals a_u and b_g, and one bridging out-of-plane molecular orbital b_g. In the D_{2h} dimer $KCuCl_3$, the mixed X,Y polarization, which indicates a lower effective symmetry C_i site, makes a direct assignment somewhat ambiguous; however, on the basis of the similar energies, band shapes, and intensities, the assignment of the dimer band in this complex should be analogous to that for the C_{2h} dimers. From correlation of C_{2h} to D_{2h}, the possible charge-transfer assignment for the dimer band is either one of the $^1B_{3u} \leftarrow {}^1A_g$ X-polarized transitions originating from the b_{1g} and b_{2u} terminal in-plane (nonbonding) molecular orbitals or one of the $^1B_{1u} \leftarrow {}^1A_g$ Z-polarized transitions originating from the a_u and b_{3g} terminal out-of-plane molecular orbitals and b_{3g} bridging out-of-plane molecular orbital.

The b_{1g} terminal in-plane molecular orbital in the D_{2h} dimer correlates to the a_{2g} in-plane nonbonding molecular orbital in the analogous D_{4h} monomer (Table VI). We have determined[10] that this orbital gives rise to the lowest energy charge-transfer transition in tetragonal mononuclear chlorocuprates; for $(C_2H_5NH_3)_2CuCl_4$, the $^2A_{2g} \leftarrow {}^2B_{1g}$ ($1a_{2g}(nb) \rightarrow 3b_{1g}$) transition is observed at 23 700 cm^{-1}. In the monomer this transition is electric-dipole-forbidden and hence would obtain its intensity purely from mixing with electric-dipole-allowed charge-transfer intensity in the dimer structure; this would lead to the strong dependence of the observed polarization of the dimer band on differences in dimer structures. Therefore, a reasonable charge-transfer assignment of the dimer band is a transition originating from this in-plane nonbonding π orbital, which has moved ~3700 cm^{-1} lower in energy in the binuclear electronic structure. Figure 7 also superimposes and compares the band shapes of the $KCuCl_3$ dimer transition and the well-resolved $^2A_{2g} \leftarrow {}^2B_{1g}$ ($1a_{2g}(nb) \rightarrow 3b_{1g}$) charge-transfer transition[10] of the mononuclear, square-planar complex dimethadonium tetrachlorocuprate(II). These two transitions are observed to have comparable band shapes, and in particular, the Huang–Rhys parameters that quantify their band shapes are similar ($S_{dimer} = 4.3$ and $S_{CT} = 3.7$; see Table IV). Thus, in contrast to the possible SPE assignment, where the dimer band is predicted to be broader than is observed, the assignment of the band as a charge-transfer transition originating from the lowest energy nonbonding π molecular orbital of the terminal chlorides is experimentally supported by the similar band shapes of the dimer transition and this charge-transfer transition in the monomer. Particularly on the basis of these band shapes, only the charge-transfer assignment for the dimer band appears reasonable.

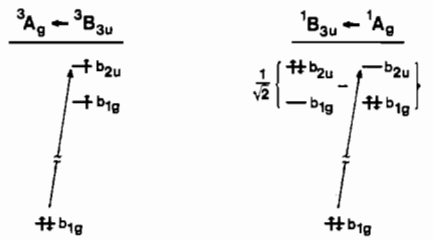

Figure 8. Spin- and parity-allowed triplet (left) and singlet (right) transitions associated with the $b_{1g} \rightarrow b_{2u}$, one-electron, charge-transfer transition. Note that the total intensity of the triplet will be ×3 due to the spin degeneracy and the total transition moment of the singlet is ×2 from the sum over the two electrons in the b_{1g} ligand orbital.

As in the previous coupled-chromophore analysis of the SPE assignment, there are four spin-allowed transitions that are predicted for a charge-transfer excitation originating from one of the dimer ligand molecular orbitals (see Table VIIB,C). For the b_{1g} orbital of $KCuCl_3$ these are the parity-allowed singlet ($^1B_{3u} \leftarrow {}^1A_g$), the parity-forbidden triplet ($^3B_{3u} \leftarrow {}^3B_{3u}$), the parity-allowed triplet ($^3A_g \leftarrow {}^3B_{3u}$), and the parity-forbidden singlet ($^1A_g \leftarrow {}^1A_g$); all four of these spin-allowed transitions might initially be expected to have similar energies. On the basis of the temperature dependence of its intensity, the main dimer band is thus assigned as the allowed singlet charge-transfer transition $^1B_{3u} \leftarrow {}^1A_g$.

At low temperature only the ^1A_g ground state of $KCuCl_3$ is populated and only transitions from this singlet can be observed. Therefore, possible assignments for the weak shoulder at ~1600 cm^{-1} higher energy (Figure 6B, top) would be the parity-forbidden $^1A_g \leftarrow {}^1A_g$ transition or the spin-forbidden $^3A_g \leftarrow {}^1A_g$ or $^3B_{3u} \leftarrow {}^1A_g$ transitions. The latter assignment, however, would indicate that the singlet–triplet splitting in this excited state is at least 1600 cm^{-1}, compared to 50 cm^{-1} in the ground state (vide infra) of $KCuCl_3$.

As the temperature is increased from 7 K, the $KCuCl_3$ dimer band intensity decreases. Yet, up to 200 K there remains a ~3000-cm^{-1} spectral window (from the dimer band up to the ~23 000-cm^{-1} sharp rise of the intense Laporte-allowed charge-transfer transitions; see Figure 6B, top) and no intensity, which would correspond to transitions originating from population of the ground-state triplet, is observed to grow in this region. Further, in $LiCuCl_3 \cdot 2H_2O$, the triplet component of the ground state is lowest in energy, yet no low-temperature triplet intensity is observed (Figure 6B, bottom) in the ~3000-cm^{-1} spectral window above the singlet dimer band, which is observed only at higher temperatures.

The intensity of the parity-allowed triplet transition $^3A_g \leftarrow {}^3B_{3u}$, relative to that of the observed singlet transition $^1B_{3u} \leftarrow {}^1A_g$, can be estimated from the relative contributions of the parity-allowed one-electron orbital changes $b_{1g} \rightarrow b_{2u}$. As indicated in Figure 8, the degeneracy-weighted intensity of the allowed triplet $^3A_g \leftarrow {}^3B_{3u}$ is $3[\langle b_{1g}||r||b_{2u}\rangle]^2$ while that of the allowed singlet $^1B_{3u} \leftarrow {}^1A_g$ is $[2(1/2^{1/2})\langle b_{1g}||r||b_{2u}\rangle]^2$, where $\langle b_{1g}||r||b_{2u}\rangle$ is the reduced matrix element of the allowed one-electron transition. The reduced matrix element cancels, and the ratio of triplet to singlet transition intensity is determined to be 3/2. Further, as indicated earlier in the discussion of the SPE assignment, any additional singlet

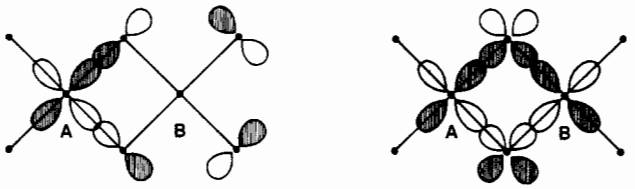

Figure 9. Half-occupied, nonorthogonal, magnetic orbitals associated with (left) the one-electron charge-transfer excited state originating from the a_{2g} ligand-centered orbital on one "half" ($Cu_BCl_4^{2-}$) of the $Cu_2Cl_6^{2-}$ dimer and (right) the ground state of the $Cu_2Cl_6^{2-}$ dimer.

intensity mechanism due to configurational interaction with the singlet Cu(II) → Cu(II) charge-transfer transition is not consistent with the observed polarizations of the dimer band.

Thus, the spin-allowed, parity-allowed triplet excitation should have an intensity comparable to that of the allowed singlet. Since this triplet band is not observed in any of the three dimers within 3000 cm^{-1} of the allowed singlet and the ground-state exchange splittings are relatively small ($<|70|cm^{-1}$), the excited-state singlet is required to be stabilized by at least 3000 cm^{-1} relative to the corresponding excited-state triplet in all three dimer salts.

Therefore, the key feature in this assignment appears to be that the dimer band is a singlet charge-transfer transition that is stabilized by several thousand wavenumbers relative to the corresponding triplet in the binuclear structure. Qualitatively this large singlet stabilization appears reasonable from the overlap of the nonorthogonal magnetic orbitals associated with each $CuCl_4^{2-}$ "half" of the dimer in the nonbonding π charge-transfer excited state (Figure 9, left). Charge-transfer excitation at one copper center (B in Figure 9) produces a hole in the a_{2g} orbital (D_{4h} monomer) extending over its four chloride ligands. The two bridging-chloride orbital components have good overlap with the d_{xy} ground state on the second copper (A in Figure 9), and this overlap should strongly stabilize the singlet excited state relative to the triplet. Alternatively, in the ground state (Figure 9, right) the overlap between two d_{xy} orbitals is mediated through nearly orthogonal p orbitals on the bridging chlorides and thus the singlet stabilization is limited and is sensitive to small structural variations. Further, as emphasized by Hansen and Ballhausen[7b] for the singlet ground state in $Cu_2(OAc)_4 \cdot 2H_2O$, configurational interaction with the lowest energy Cu(II) → Cu(II) charge-transfer transition ($d_{xy} \rightarrow d_{xy}$) can also contribute significantly to stabilization of this charge-transfer excited-state singlet. This metal-to-metal transition has been thought to be at energies >100 000 cm^{-1}. However, recent experiments[31] on NiO with photoelectron and bremsstrahlung isochromat spectroscopies have indicated that this transition might actually be at much lower energy because of a large decrease in electron–electron repulsion due to covalent delocalization. From variable-energy photoemission spectroscopy we have, in fact, observed[32] that, for $CuCl_4^{2-}$, ionization of a valence Cu(II) electron results in a lowest energy final state that involves one hole on the Cu and the second hole on the ligand. This state is observed to be ~8 eV lower in energy than the pure Cu d^8 final state, and this stabilization derives from a large orbital relaxation that lowers electron–electron repulsion.

In summary, this study has provided an experimental assignment of the binuclear cupric dimer band as a singlet nonbonding π ligand-to-copper charge-transfer transition that is several thousand wavenumbers lower in energy than the corresponding triplet transition. Further studies, however, are required to more quantitatively evaluate the electronic structural contributions to this stabilization of the singlet charge-transfer transition in the dimer structure.[33]

Finally, with respect to the electronic origins of "dimer bands" in other binuclear cupric complexes, an analogous singlet charge-transfer assignment must also be appropriate for copper carboxylates on the basis[4b] of the temperature dependence of the intensity of the 360-nm band in $Cu_2(OAc)_4 \cdot 2H_2O$. Detailed spectral studies are still required, however, to define the electronic structural origins of low-energy bands in other cupric dimers (e.g. Cu^{II}–L–Cu^{II}, where L = hydroxide, alkoxide, or phenoxide).

Acknowledgment. We are grateful to the National Science Foundation (Grant NSF-CHE 8204841; E.I.S.) and the Research Corp. (R.L.M.) for support of this research. S.R.D. thanks the "Direction generale de l'enseignement superieur" of the Province of Quebec for support, and R.L.M. acknowledges H. E. Bunting for assistance with the reflectance experiments.

Registry No. 3, 72268-09-8; $Cu_2Cl_6^{2-}$, 16969-70-3; $(CH_3NH_3)_2CuCl_4$, 16950-47-3; $(C_2H_5NH_3)_2CuCl_4$, 16950-48-4; $(N(2amet)pipzH_3)CuCl_5 \cdot 2H_2O$, 95463-74-4; $KCuCl_3$, 13877-25-3; NH_2CuCl_3, 17169-54-9; $LiCuCl_3$, 38581-59-8.

(31) (a) Sawatzky, G. A.; Allen, J. W. *Phys. Rev. Lett.* **1984**, *53*, 2339–2346. (b) Fujimori, A.; Minami, F. *Phys. Rev. B: Condens. Matter* **1984**, *30*, 957–971.

(32) Cohen, S. L.; Didziulis, S. V.; Gewirth, A. G.; Solomon, E. I., to be submitted for publication.

(33) We note that a recent Xα–SW study on $Cu_2Cl_6^{2-}$ (Bencini, A.; Gatteschi, D., private communication) calculates the lowest energy, broken-symmetry, charge-transfer transition to be at 3555 cm^{-1} lower energy than the lowest energy charge-transfer transition in the $CuCl_4^{2-}$ monomer.